



Contents lists available at ScienceDirect

Ore Geology Reviews

journal homepage: www.elsevier.com/locate/oregeo

Ta and Sn concentration by muscovite fractionation and degassing in a lens-like granite body: The case study of the Penouta rare-metal albite granite (NW Spain)



Francisco Javier López-Moro^{a,b,*}, Francisco García Polonio^{a,b}, Teresa Llorens González^{a,b}, José Luis Sanz Contreras^c, Agustina Fernández Fernández^b, María Candelas Moro Benito^b

^aStrategic Minerals Spain, S.L., P^o Recoletos, 37, 28004 Madrid, Spain

^bDpt. of Geology, University of Salamanca, Plaza de los Caídos s/n, 37008 Salamanca, Spain

^cDpt. of Geological and Mining Engineering, School of Mining and Energy Engineering, Technical University of Madrid, C/ Ríos Rosas, 21, 28003 Madrid, Spain

ARTICLE INFO

Article history:

Received 29 July 2016

Received in revised form 18 November 2016

Accepted 20 November 2016

Available online 25 November 2016

Keywords:

Fractional crystallisation

Ta/Nb ratio

Degassing

Central Iberian Zone

ABSTRACT

The Penouta peraluminous low-phosphorous granite is the most important low-grade, high-tonnage Sn-Ta-Nb-bearing albite granite from the Iberian Massif. A sheet or laccolith shape, instead of a stock, is inferred for the Penouta granite, maybe in relation with the low viscosity and high mobility of a fluorine-bearing melt. Subhorizontal lateral extension of the magma is also inferred via vertical and horizontal geochemical variations. The absence of compositional gaps in variation diagrams, coupled with continuous evolutionary trends of compatible and incompatible elements with height, discard a multi-pulse intrusion and point to a single magma pulse. Mineral chemistry, trace element and least-squares mass balance modelling support a differentiation process from bottom to top in the emplacement place. The absence of switch from incompatible to compatible behaviour (bell-shaped trends) in Sn, Nb and Ta variation diagrams, coupled to experimental constraints on tantalite and cassiterite saturation, suggest that Nb-Ta oxides and probably cassiterite were not fractionated mineral phases, their crystallisation being related to concentration gradients within a trapped intercumulus melt. Major and trace element modelling support that the concentration upwards of Ta and the Ta/Nb ratio could be a consequence of mineral fractionation, with a key role of muscovite (mainly primary) for the Ta/Nb ratio, as this mineral has a higher partition coefficient for Nb than Ta. Our results suggest that fluorine and peraluminosity had a limited effect in the Ta/Nb ratio variations. Hence, Ta enrichment is mainly controlled by fractional crystallisation processes. In most cases, Sn enrichment was also concomitant with Ta, indicating that crystal-melt fractionation processes also played an important role in Sn concentration. Nevertheless, the strongest Sn enrichment in the granite (e.g., central part of the granite body) does not correspond to a significant Ta enrichment. The high affinity of Sn for fluids and the high partitioning of Ta for melt could explain this decoupling. Nevertheless, the magmatic signature of cassiterites in these strongly Sn-enriched zones (central part of the granite body) rules out a hydrothermal subsolidus origin for this fluid. By analogy with models carried out in sill-like bodies it seems likely that the Sn enrichment in the central part of the granite body is related to fluid saturation/degassing occurred in the lower margin, as a consequence of cooling and crystallisation of mostly anhydrous minerals (i.e. second boiling). The vapour exsolved migrated into the hotter melt up to the central part, where it probably was reabsorbed, yielding cassiterite with a magmatic signature. Moreover, we suggest that heat loss in the upper margin of the granite body might also contribute to the formation of a second fluid-saturated zone. As a result, pegmo-aplites and greisen were developed.

© 2016 Elsevier B.V. All rights reserved.

1. Introduction

It is commonly accepted that Ta-mineralised granites correspond to volatile-enriched melts obtained by extreme degrees of chemical fractionation (Cuney et al., 1992; Lehmann, 1994;

* Corresponding author at: Strategic Minerals Spain, S.L., P^o Recoletos, 37, 28004 Madrid, Spain.

E-mail address: jlopez@strategicminerals.com (F.J. López-Moro).

Charoy and Norohna, 1996; Helba et al., 1997; Huang et al., 2002; Linnen and Cuney, 2005; Černý et al., 2015; Küster, 2009; Canosa et al., 2012). In line with this assertion these granites can occur along with other less evolved granitoid intrusions (granodiorites, biotite granites, or two mica granites) that could be their precursors (see Küster, 2009; Canosa et al., 2012). In other cases, albite granites appear to be as isolated bodies, but commonly in upper crustal levels, such that they may represent the most allochthonous batch of granite magma at regional scale (e.g., Golpejas albite granite, Arribas et al., 1982). The latter begs the question of whether these melts suffered an extreme differentiation process “en route” to the surface, because the precursor magma remains, a priori, unknown. Alternatively, it has recently been suggested that albite granites could be formed by melting of plagioclase-rich layers (Barbony and Bussy, 2013), a very attractive hypothesis but poorly constrained yet.

Rare-metal-bearing albite granites content high amount of fluxing components, which not only facilitate fractional crystallisation, but also reduce the viscosity of these magmas (Linnen and Cuney, 2005). A consequence of low-viscosity magmas is their tendency to be emplaced in tabular bodies, as is the case of diabase sills (e.g. Woodruff et al., 1995; López-Moro et al., 2007) or two mica granites with fluxing elements (López-Moro et al., 2012; Chicharro et al., 2015). Therefore, it is expected that rare-metal-bearing albite granites exhibit laminar shapes, as it has especially been attributed to some albite granites with a restricted thickness, namely the Golpejas albite granite (Arribas et al., 1982), the Nuweibi albite granite (Helba et al., 1997), or albite granites from St-Jean-du-Doigt intrusion (Barbony and Bussy, 2013), although small stocks have also been reported (e.g. Argemela albite granite, Charoy and Norohna, 1996; or the Penouta albite granite itself, Mangas and Arribas, 1987).

Many efforts have been undertaken to try to decipher the relationships between the ore distribution and the hosting albite granites. Nevertheless, how the concentration of tantalum relative to niobium is achieved is an open issue, but some factors have been proposed, namely, crystallisation of columbite (Chevychev et al., 2010; Černý et al., 2012), the occurrence of fluxing elements like fluorine (e.g. Bartels et al., 2010), high alumina saturation index in the melt (van Lichtenvelde et al., 2010; Fiege et al., 2011), fractional crystallisation coupled to subsolidus hydrothermal or orthomagmatic fluids (Dostal et al., 2015; Ballouard et al., 2016) or micas as fractionated phases (Raimbault and Burnol, 1998; Stepanov et al., 2014). In this regard, a granite body with a relatively simple emplacement and crystallisation history would provide an excellent field laboratory to get constraints about chemical variations from bottom to top and check these hypotheses.

The availability of several deep drill holes in the Penouta granite, widely sampled for whole-rock and mineral chemistry, allows to gain insight into the intrusion history and the evolution of this kind of melts and the ore, in a similar fashion to classical modelling for zoned pegmatite fields (e.g. Černý, 1989). Detailed geochemical and mineralogical profiles will permit us to approach the mechanism of emplacement: multi-intrusion (e.g., Cuney et al., 1992; Yin et al., 1995) or a single pulse. The mechanism of differentiation and how Ta relative to Nb is concentrated in the granite body are addressed. We also deal with the role played by vapour released from the magma in Sn concentration and subsolidus overprints.

2. Geological setting

All Variscan rare-metal-bearing granites from the Iberian Massif are located in the innermost part of the Iberian Variscan Belt, a domain known as the Central Iberian Zone (CIZ) (Fig. 1), which is

equivalent to the South Armorican Zone, the French Central Massif and the Moldanubian Zone. In these internal domains the collision of Gondwana with Laurentia led to the Proterozoic Gondwanan basement of Cadomian (West African) affinity that was overlain by Palaeozoic passive margin sequences, mainly siliciclastic (e.g. Fernández-Suárez et al., 2002; Gutiérrez-Alonso et al., 2005). From a metallogenetic point of view, the CIZ could be considered as the southwest extension of the Sn-W metallogenetic province of the European Variscan Belt.

Based on tectonostratigraphic criteria, the CIZ has been divided in two main domains (Martínez-Catalán et al., 2004): the Ollo de Sapo Domain (OSD) and the Schist Greywacke Complex Domain (SGCD). In the OSD latest Cambrian to Early Ordovician subvolcanic, volcanic and volcano-sedimentary rocks (Ollo de Sapo Formation, see Díez Montes et al., 2010) crop out in recumbent folds with northeast vergence. In contrast, the SGCD consists of a metasedimentary turbidite sequence (e.g. Rodríguez-Alonso et al., 2004) that surfaces in upright folds. Considering the augen gneisses as intrusives equivalent to the volcanic materials of the Ollo de Sapo Formation, most Variscan rare-metal-bearing granitoids from the Iberian Massif are located in the OSD, except for the Trasquilón granite (Fig. 1).

In the Central Iberian Zone, the Variscan orogeny generated most of the structures, the internal deformation, and the metamorphism. Overturned to recumbent folds with northeast vergence in the OSD and vertical folds in the SGCD were produced during the D₁, in both cases with a low-grade slaty cleavage (S₁) dated between 359 Ma and 336 Ma (⁴⁰Ar/³⁹Ar; Dallmeyer et al., 1997). The Variscan D₂ phase yielded thrusting toward the external zones, whereas in the middle and lower parts extensional events triggered crustal anatexis and a pervasive subhorizontal tectonic foliation (S₂). Thrusting has been dated between 343 and 321 Ma (Dallmeyer et al., 1997), ages that roughly overlap with the extensive migmatization event (325–311 Ma, U-Pb in monazites, see Valverde-Vaquero et al., 2007; Díez Montes et al., 2010). The Variscan D₃ phase is characterised by upright folds, open-to-tight folds and occasionally a crenulation cleavage (S₃). Other D₃ Variscan structures are the subvertical strike-slip shear zones with mostly dextral wrench components. D₃ stage folds the metamorphic isograds and the S₂ foliation of the deepest zones. An age between 315 and 306 Ma constrains this deformation stage according to the ages of granitoids of this phase and subvertical strike-slip shear zones (e.g. Valle-Aguado et al., 2005; López-Moro et al., 2012; Gutiérrez-Alonso et al., 2015).

The Penouta granite is located in the OSD, in a large structure, the Ollo de Sapo Anticlinorium, which is characterized by the presence of two formations: the Viana do Bolo Series and the Ollo de Sapo Formation (Fig. 1). The Viana do Bolo Series (Early Cambrian) consists of highly metamorphosed rocks, including banded migmatitic gneisses, garnet-bearing schists, marbles, calc-silicate rocks and scarce amphibolites, but only the two first crop out close to the Penouta granite (Fig. 1). Furthermore, close to the Penouta mine orthogneisses appear intercalated in the Viana do Bolo Series (Ramilo orthogneiss). The protolith of this orthogneiss was a medium- to coarse-grained biotitic porphyritic granitoid, which intruded into the Viana do Bolo Series and the whole was intensively metamorphosed and often migmatized during the Variscan orogeny. The Ramilo orthogneiss is undated, although other equivalent orthogneisses (Covelo and San Sebastian orthogneisses) yielded ages of 487 ± 4 Ma and 470 ± 3 Ma, respectively (Montero et al., 2009). The Ollo de Sapo Fm. (495–483 Ma, Díez Montes et al., 2010) overlies the Viana do Bolo Series. It consists of augen gneisses, epiclastic tuffs and ignimbrites, but only the augen gneiss partially migmatized surfaces nearby the Penouta granite (Fig. 1).

There are no available ages from the Penouta granite and only a relative time can be inferred from structural and contact relation-

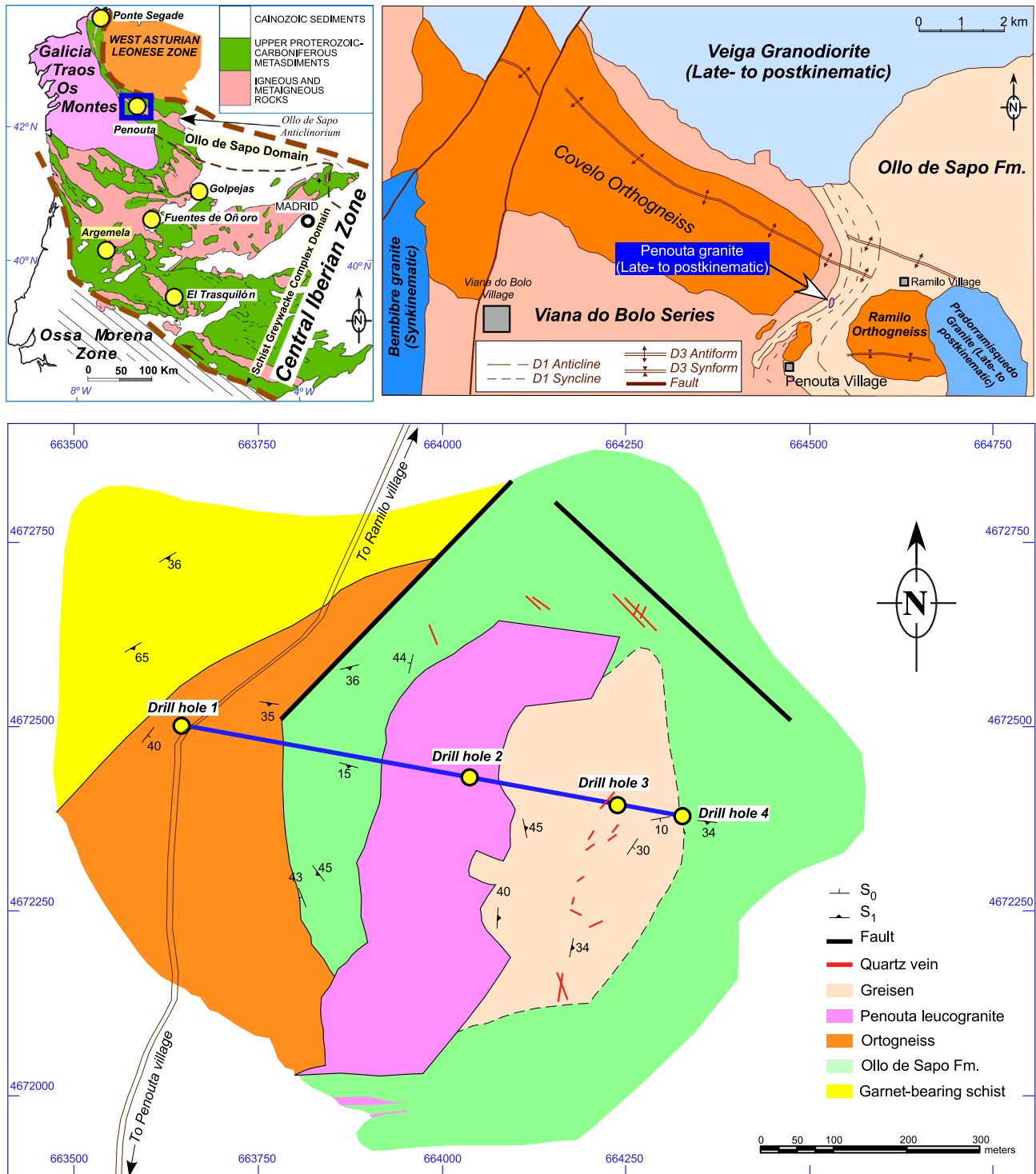


Fig. 1. Upper left: Geological map of the Central Iberian Zone including the most important rare metal-bearing albite granites (yellow spot). Upper right: Geological sketch of the Ollo de Sapo Anticlinorium in its western region (modified from IGME, 1982). Down: Detailed geological map of the Penouta granite with the location of the selected drill holes. (For interpretation of the references to colour in this figure legend, the reader is referred to the web version of this article.)

ships. The lack of foliation and significant internal deformation in this body are typical features of a late- to post-Variscan character. Similar structural features have also been reported in other granitoids of the area, as Veiga and Pradorramisquedo plutons (Fig. 1), which have been related to a strike-slip shear zone (Vegas et al., 2001), this stage being similar in age (c. 308 Ma, Gutiérrez-Alonso et al., 2015) to other Sn-bearing granites recently dated in

the CIZ (e.g. Logrosán Sn-(W) ore deposit, 308 ± 1 Ma, Chicharro et al., 2015).

3. Sampling methodology

Sampling was mainly carried out from four exploration drill cores of 250 m in thickness, among more than 50 drilling sections.

Drill cores selected follow a hypothetical line that transects the granite from E to W. The reasons for choosing these sections were as follows: i) there are topographical variations among the sections, since eastern ones are at a higher topographic level, allowing the study of a higher vertical section of the granite body, ii) there are petrological differences, with the occurrence of flat-lying sheets of aplo-pegmatite sandwiched with the granite at the apical side of the granite in the drill holes from the East, that are missing in western sections, iii) there are mineralogical differences, with more quartzose and micaceous granite facies in the western drill core, iv) there are geochemical differences, since the highest contents in Ta are at the eastern drill holes. Differences among the selected 4 drilling sections are the clue to unravel the differentiation processes involved in the evolution of the Penouta granite and its associated mineralization.

For exploration purposes every drill core was completely sampled, collecting the half of the core every 2.5 m. However, for research purposes those samples with quartz-veins, strongly weathered or containing fragments from the country rock were discarded, in order to consider only rocks representing the composition of the pristine magma. Data consist of a complete set of trace elements (Table 1), including REE, and a more restricted set of major elements, the latter sampled every 10 m, except for drill hole number 3 that was sampled entirely for major elements.

4. Geology of the Penouta granite

The drill holes carried out for exploration allow to constrain the shape and size of the Penouta granite (Fig. 2). Some of the drill holes cut the metamorphic rocks at the bottom of the granite, which leads to infer a lens-like shape of this body. Similar shapes (from inflated sills up to laccoliths) have been constrained in leucogranites with fluxing elements of central-western of Spain and this fact appears to be a rule in this granite types. The Penouta granite outcrops in an area of around 0.2 km² and in the current state of outcrop (strongly influenced by the old mining works) it is elongated in the north-south direction (Fig. 1), as it is also the case of the Pradorramisquedo pluton. The Penouta leucogranite was emplaced in the hinge of a D₁ Variscan antiform (Fig. 1), an ideal scenario where the uprising magma has sufficient room where it can be emplaced, avoiding the “room problem”. The study of outcrops and drill core sections supports that the granite intruded following planar anisotropies, mainly the foliation of the Ollo de Sapó Fm. and orthogneisses of the Viana do Bolo Fm. This granite developed, especially in the Eastern zone (Fig. 1), a Sn-enriched greisen in overlain metamorphic rocks.

Differences in the colour of hand specimens occur from the top to the bottom of the granite. The greenish colour becomes more intense at the bottom. Granites of the apical zone are always leucocratic and fine-grained in hand specimen. This is the part of the granite where kaolinite is more abundant, providing the whitish colour at different extent, depending on its abundance. More in depth, when the kaolinite content decreases or disappears the granite displays a pale green colour, mainly by the colour of the white mica, that changes to a darker green in the deepest levels (e.g. samples of drill hole 1), where the white mica also exhibits a darker green colour. No relevant changes in grain size occur in the whole granite body, but the finest-grained granite occurs at the apical zone, specifically in the contact with the country rock, which could be interpreted as a chilled margin. Gradational margins or contacts of different magma pulses were not observed. The granite margin is the only place with a significant orientation of plagioclase laths (concordant with the country rock), although without deformation, suggesting a flow of magma adjacent to the wall of country rock and a low viscosity of the magma. The lack of orientation in the rest of the granite is interpreted to be the

result of a rapid magma emplacement followed by crystallisation after magma flow, in a similar fashion as it has been reported in flood basalts (e.g. Philpotts and Ague, 2009).

Occasionally, flat-lying sheets of aplo-pegmatite can be found in the Penouta granite, specifically occurring in the apical zone. These structures are nearly horizontal tabular bodies with centimetric to metric thick, composed by different proportions of the main constituents (e.g.: quartz-mica layers, albite layers and quartz layers) rhythmically sandwiched.

The Penouta Sn-Ta-Nb-bearing granite exhibits a disseminated mineralization of cassiterite and columbite-tantalite, indicating a passive crystallisation of the magma, in contrast with B-bearing magmas that provide evidence of explosive processes such as formation of breccia pipes and stockworks (Pollard et al., 1987). The columbite-tantalite and the cassiterite occur from bottom to the top, respectively, of the granite body with the highest abundances in the apical zone (see below) and cassiterite occasionally is also enriched at mid-levels. Furthermore, a hydrothermal episode occurred developing a stockwork of veins up to 2 m in thickness developed in the Ollo de Sapó Fm. (Fig. 1) and smaller and tabular in shape veins not thicker than 30 cm in the granite. The stockwork is composed of sigmoidal, lenticular and tabular in shape hyaline to milky quartz veins with cassiterite mineralization. The veins are mainly composed of quartz, although barite, sphalerite, galena, chalcopyrite, pyrite and bismuthinite can also occur.

5. Petrography and mineral chemistry

Mineralogically, plagioclase, quartz, potassium alkali feldspar and white micas are essential minerals in all the granite types (Table 2), whereas garnet, cassiterite, apatite, beryl, monazite, zircon, columbite-tantalite and uraninite are accessory minerals almost ubiquitous. Biotite and topaz are missing in all the granite facies. Other rare accessory minerals are fluorite and microlite and occasionally sulphide minerals can also occur, either in nodules or, more frequently, related to small veins. Sphalerite, galena, arsenopyrite, pyrite, bismuthinite, chalcopyrite and stannite are the most common sulphides.

Quartz mainly occurs in euhedral to anhedral phenocrysts from 1 mm up to 3 mm in size that include minute albite laths arranged concentrically along growth planes, commonly known as “snowball” quartz. This quartz type has a magmatic origin and its occurrence is a distinctive feature of rare metal-bearing leucogranites (e.g. Pollard, 1989; Helba et al., 1997). The highest contents are in the western drill hole (34.7 wt% on average, Table 2) lowering up to 21.9 wt% in eastern drill holes.

Albite is an ubiquitous mineral in all granite facies, with abundances that reach up to 53 wt% on average in the eastern drills, and only a 37 wt% on average in the deepest sections. Albite occurs in three forms: (i) laths of euhedral crystals included in quartz and potassium alkali feldspar phenocrysts, with sizes not more of 0.5 mm, (ii) laths of euhedral to subhedral crystals forming the groundmass, with variable size depending the location of the sample, with sizes not more than 0.5 mm in the apical zone and up to 1 mm in deeper samples, and (iii) crystals replacing potassium alkali feldspars, which are found locally in the apical zone. Type ii is by far the most abundant albite type. In a similar fashion to others albite granites (e.g. Nuweibi granite, Helba et al., 1997) plagioclase laths are aligned parallel to the contact with the host rock in the apical zone. Microprobe analyses of all albite types revealed a restricted compositional variation (Ab₉₇₋₉₉).

Potassium-feldspar (11.9–17.2 wt% on average) mostly occurs as large unzoned and subhedral crystals (up to 2.8 mm in size), with albite inclusions in the biggest K-feldspar crystals, and some of them seem to be replaced by secondary albite. Smaller crystals

Table 1
Whole-rock chemical composition, liquidus estimates and tetrad effect of representative analyses of the drill holes studied.

Sample Hole Depth (m)	D.L.	D05530 1	D06053 1	D05007 2	D05249 2	D05255 2	D02666 3	D02744 3	D02944 3	D02972 4	D02990 4	D03290 4
SiO ₂ (wt%)	0.01	76.1	75.4	76	77.1	75.8	72.2	74.9	75	70.8	76.4	73.8
TiO ₂	0.01			0.005	0.005	0.005						
Al ₂ O ₃	0.01	14.3	14.25	15.25	15	15.45	15.9	15.9	15.25	16.6	15.25	15.6
Fe ₂ O _{3t}	0.01	0.93	1.12	0.78	0.84	0.95	0.32	0.4	0.45	0.55	0.78	0.66
MnO	0.01	0.03	0.03	0.03	0.05	0.04	0.02	0.04	0.03	0.02	0.04	0.14
MgO	0.01	0.03	0.03	0.03	0.02	0.02	0.03	0.02	0.03	0.03	0.01	0.02
CaO	0.01	0.11	0.13	0.1	0.13	0.14	0.16	0.14	0.13	0.14	0.14	0.15
Na ₂ O	0.01	4.43	4.33	5.26	4.98	5.99	6.67	6.31	5.72	6.3	5.51	6.22
K ₂ O	0.01	3.48	3.83	3.6	4.07	3.39	3.43	3.49	3.58	3.55	3.35	3.36
P ₂ O ₅	0.01	0.05	0.04	0.02	0.04	0.04	0.06	0.06	0.05	0.07	0.06	0.06
LOI	0.01	n.d.	n.d.	n.d.	n.d.	n.d.	0.81	0.68	0.64	n.d.	n.d.	n.d.
Total		99.46	99.16	101.08	102.24	101.83	99.60	101.26	100.88	98.06	101.54	100.01
A/CNK		1.20	1.23	1.15	1.09	1.10	1.05	1.10	1.08	1.12	1.14	1.08
Cs (ppm)	0.01	35.1	25.0	50	28.9	24.9	33.3	36.6	28.3	42.1	47.9	48.6
Rb	0.2	939	846	1080	972	810	833	949	792	962	960	881
Ba	0.5	68	36.6	2.2	5	6.4	19.9	2	31.3	91.9	1.5	2.2
Sr	0.1	18.1	6.3	3.7	14.3	15.2	31.6	4	22.5	62.6	7.3	9
Ga	0.1	35.5	36.4	35	29.8	30.6	34.1	36	29	36.6	37.3	32.5
Cr	10	–	–	–	–	–	10	–	–	10	10	10
Zr	2	27	27	28	25	30	20	22	17	13	15	20
Hf	0.2	5.5	4.7	6.4	5.5	6.2	8.1	7.1	5.3	7.8	7.3	7.5
Sn	1	103	90	273	46	46	902	312	194	813	513	222
Nb	0.2	72	49.1	75.3	71	68.7	80	52.8	55.2	88.6	68.6	65.2
Ta	0.1	46.2	20	65.1	40.7	38	130	95.6	39.3	158.5	99.7	87.3
Th	0.05	2.87	3.09	2.41	2.81	3.17	2.91	2.61	2.16	2.16	2.63	2.44
Tl	0.5	4	3.5	5	4.6	3.8	4	4.8	3.8	4.9	4.9	4.6
U	0.05	15.8	12.1	2.02	8.66	14.15	10	14.95	10.15	6.77	9.71	11.55
W	1	2	3	2	3	3	2	2	2	4	2	2
Y	0.5	4.6	7.4	3.5	6.4	5.7	2	3.2	3.6	1	2.7	2.9
La	0.5	1.1	1.8	0.8	1.4	1.2	0.7	0.7	0.8	–	0.5	0.6
Ce	0.5	2.8	5.1	2.2	3.7	3.4	1.6	1.7	2.2	0.7	1.2	1.7
Pr	0.03	0.46	0.72	0.34	0.55	0.49	0.21	0.26	0.31	0.09	0.19	0.27
Nd	0.1	1.7	3.1	1.4	2.2	2	0.8	0.9	1.3	0.3	0.8	0.9
Sm	0.03	2.96	4.2	2.23	3.46	3.1	1.06	1.97	2.33	0.46	1.44	1.92
Eu	0.03	–	–	–	0.03	–	0.03	–	0.03	0.09	–	–
Gd	0.05	6.37	8.31	4.77	6.72	5.63	2.27	4.27	4.15	0.94	3.14	4.18
Tb	0.01	1.1	1.32	0.92	1.31	1.06	0.45	0.81	0.89	0.21	0.67	0.8
Dy	0.05	2.29	3.45	1.79	2.88	2.38	0.92	1.57	1.7	0.44	1.31	1.51
Ho	0.01	0.05	0.11	0.05	0.07	0.07	0.03	0.03	0.05	0.02	0.02	0.04
Er	0.03	–	0.03	–	0.04	0.04	0.03	–	0.1	0.04	–	–
Tm	0.01	–	–	–	–	–	–	–	–	0.01	–	–
Yb	0.03	–	–	–	–	–	0.04	–	0.08	0.08	–	–
Lu	0.01	–	–	–	–	0.01	0.01	–	0.01	0.01	–	–
ΣREE		19	28	15	22	19	8	12	14	3	9	12
Zr/Hf		4.9	5.7	4.4	4.5	4.8	2.5	3.1	3.2	1.7	2.1	2.7
T _{Zrn} (°C)		668	665	664	656	663	630	641	627	609	623	634
T _{Mnz} (°C)		654	676	627	650	634	574	602	614	–	596	600
TE ₁₋₃		1.9	1.7	1.8	1.9	1.8	1.7	2.0	1.8	–	2.1	1.9

Whole-rock analyses were performed at the ALS in Canada. Major element analyses were carried out by using the ME-ICP06 package, consisting of a sample decomposition with Lithium Metaborate/Lithium Tetraborate (LiBO₂/Li₂B₄O₇) fusion and the resulting product was analysed by inductively coupled plasma-atomic emission spectrometry (ICP-AES). Trace elements and REE were determined by using the ME-MS81 Ultra-Trace Level package, with the same sample decomposition method as major elements, whereas the product was analysed by inductively coupled plasma-mass spectrometry (ICP-MS). D.L.: Detection limit; LOI: Loss on ignition; n.d.: not determined; A/CNK: molar Al₂O₃/(CaO + Na₂O + K₂O); –: below detection limit; T_{Zrn} and T_{Mnz}: estimates of liquidus temperatures from zircon and monazite saturation models after [Watson and Harrison \(1983\)](#) and [Montel \(1993\)](#), respectively; TE₁₋₃: tetrad effect quantification as the TE₁₋₃ parameter from [Irber \(1999\)](#).

(around 300 μm) also occur in the groundmass. K-feldspars and quartz form the largest crystals of the granite that are mainly surrounded by albite of the groundmass. Vein, string or patch perthites are frequent. A cloudy aspect is not uncommon due to the occurrence of kaolinite. The compositional variation ranges from Or₉₂ to Or₉₈, with the highest contents close to patch perthites, where the K-feldspar is cleaner, suggesting Na unmixing in subsolidus conditions.

White micas occur in large subhedral flakes or small anhedral to subhedral flakes. Differences in colour of white micas are exhibited from top to bottom, with darker green colours at deeper levels. Electron-microprobe data reveal that phengites and muscovites exist. White micas with the darker green colours of the western drill hole resulted to be Fe-enriched ([Table 3](#)), whereas pale green

micas from the apical granites and from the greisen were Mg-enriched relative to darker ones. Most of white micas are primary according to the compositional criteria of [Miller et al. \(1981\)](#), except for white micas from the apical part that seem to be secondary, in a similar fashion than white micas from the greisen ([Fig. 3](#)). There are variations in their abundance, with 19 wt% in deeper areas and around 4 wt% in shallow levels ([Table 2](#)).

Garnet is a ubiquitous accessory mineral that commonly is transformed to white micas. Microprobe analyses of garnets from granites of the eastern and western sections show composition of Sp₇₉₋₄₄Alm₅₁₋₁₃, other components (grossular and pyrope) being very restricted ([Table 4](#)). Most of garnets are spessartite-almandine and in lesser extent almandine-spessartite. Garnets with the highest almandine components are in the deepest sample

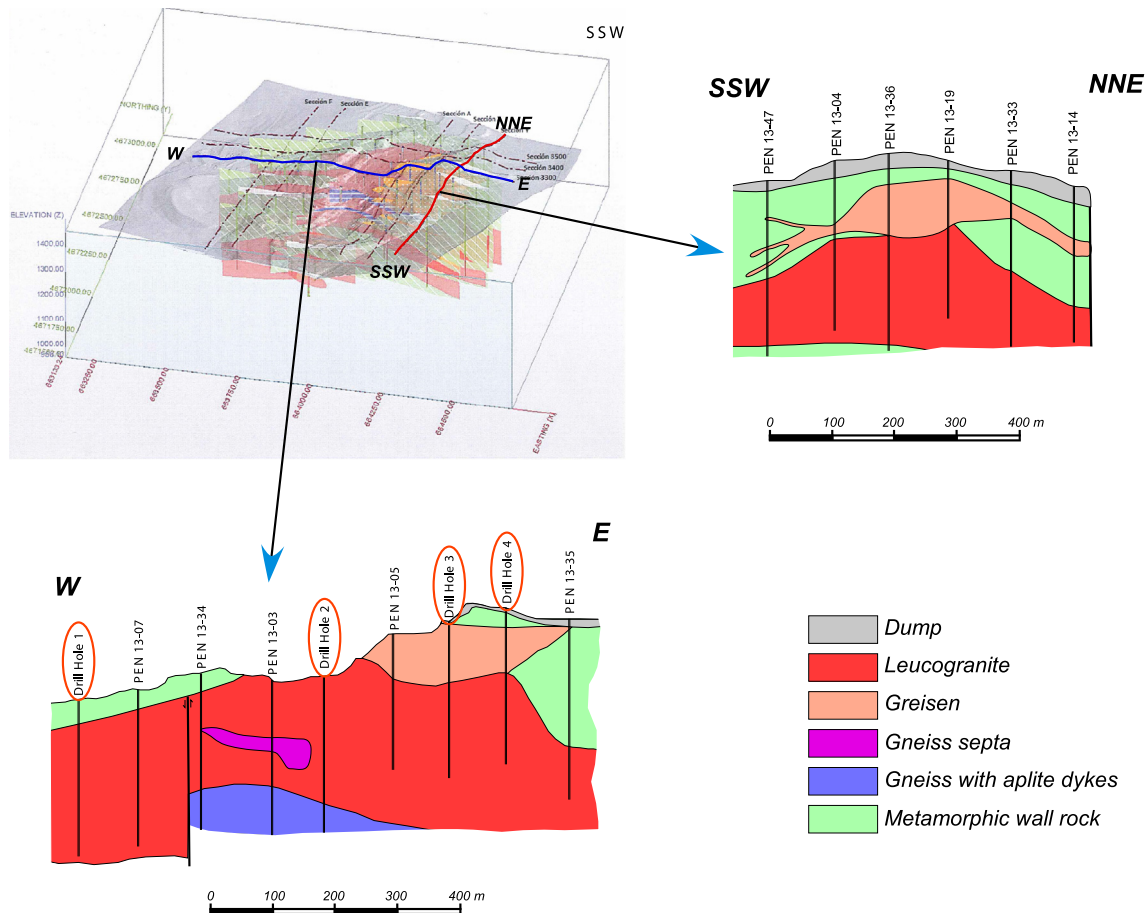


Fig. 2. Longitudinal and transversal sections in the Penouta granite constrained from drill cores.

Table 2

Average mineral abundances in selected drill holes.

Drill hole/location	Quartz (wt%)	Albite (wt%)	K-feldspar (wt%)	Muscovite (wt%)	Garnet (wt%)
1/Western zone (n = 7)	34.7	36.7	13.4	14.3 (19–11)	0.73
2/Central zone (n = 6)	32.5	41.5	11.9	13.9	0.17
3/Eastern zone (n = 10)	21.9	53.4	17.2	6.83 (14–4)	0.16

n: Number of samples; numbers in brackets: range of abundances from bottom to top in the granite body; the estimations were carried out using the MINSQ code (Herrmann and Berry, 2002).

($\text{Alm}_{51}\text{Sp}_{44}$), whereas spessartite dominates in upper levels. Moreover, garnet is more abundant in depth (0.73 wt%) than in upper levels (0.16 wt%; Table 2).

Zircon always shows a cloudy and porous aspect and quadratic and prismatic sections are the rule. No zoning has been observed. Zircons of eastern and western sections exhibit differences in terms of HfO_2 contents, with the lowest contents in Hf (zircon s. s.) in the deepest levels (9.2 wt% of Hf_2O , Table 1A), that increase with the topographic level (16.6 wt% of Hf_2O , Table 1A, i.e., zircon with Hf, according to Correia Neves et al., 1974). Zircons with similar HfO_2 contents have been found in Sn and Nb-Ta-bearing albitised granites (Huang et al., 2002; Canosa et al., 2012).

Apatite is another scarce accessory mineral in the Penouta granite, although it can be quite abundant in the greisen. Fluorapatite is the dominant type, with F values ranging between 0.84 and 0.46 a.p.f.u. and with the highest contents in the apical zone. A fluorine zoning was observed in apatite crystals, with cores depleted in F relative to rims.

Monazite is a rare accessory mineral in the Penouta granite, but it has also been found in the orthogneiss host rock. Monazite of the deepest levels of the granite and that of the wall rock show prismatic crystals, whereas a rare monazite in fibrous radiate crystals can occur in the upper levels of the granite. There are differences among monazites from the granite and wall rock, with the highest contents in LREE and Th in monazites of the latter, but higher contents in Gd in the monazite of the former. Moreover, monazites of the granite shows lower LREE contents upwards (Table 2A).

Beryl is a ubiquitous accessory mineral phase in the whole granite. It also occurs in the greisen and can also be profuse at mid-levels of the western section, in close association with cassiterite (Fig. 4). Beryl occurs as euhedral to anhedral crystals with a fine- to coarse-grained size and plenty of microinclusions. Shallower beryls are sodium beryls ($\text{Na}_2\text{O} > 0.5\%$) and deeper ones sodium-lithium beryl.

Fluorite is a very rare accessory mineral and only has been found in granite facies of the upper levels of the granite in contact

Table 3
Representative compositions of white micas from the Penouta granite and greisen.

Drill hole/location	1	3	4	12-02	Open pit	Greisen
Number of data (n)	15	11	5	12	2	2
Dept from the granite upper level (m)	98–211	1–31	63	115	50	
SiO ₂ (wt%)	45.89	46.15	46.26	47.37	46.89	47.81
TiO ₂	0.004	0.056	0.013	0.010	0.021	0.066
Al ₂ O ₃	32.09	32.53	33.47	31.74	33.74	31.53
FeO	4.100	2.920	2.760	3.290	3.120	3.610
MnO	0.232	0.271	0.329	0.236	0.249	0.396
MgO	0.008	0.348	0.005	0.014	0.081	0.329
CaO	0.004	0.056	0.013	0.015	0.017	0.008
Na ₂ O	0.275	0.260	0.262	0.191	0.257	0.195
K ₂ O	10.74	10.71	10.76	10.50	10.37	10.60
P ₂ O ₅	0.005	0.004	0.006	n.d.	0.006	0.003
F	0.526	0.476	0.395	0.486	0.499	1.076
Cl	0.004	0.007	0.009	0.009	0.006	0.08
Rb ₂ O	0.655	0.715	0.560	0.645	0.348	0.542
BaO	0.002	0.006	n.d.	0.004	0.030	0.011
Sum	94.54	94.46	94.83	94.51	95.58	96.27
Si apfu	6.220	6.240	6.220	6.380	6.220	6.300
Al	5.120	5.180	5.300	5.040	5.280	4.900
Fe	0.465	0.330	0.310	0.370	0.346	0.399
Mg	0.002	0.070	0.001	0.003	0.002	0.007
Ti	0.000	0.006	0.001	0.001	0.002	0.007
Mn	0.027	0.031	0.038	0.027	0.028	0.044
Na	0.072	0.068	0.068	0.050	0.066	0.050
Ca	0.001	0.000	0.001	0.002	0.002	0.001
K	1.856	1.846	1.845	1.800	1.760	1.780
Ba	0.000	0.000	–	0.000	0.002	0.001
P	0.001	0.000	0.001	–	0.001	0.000
Rb	0.057	0.062	0.048	0.056	0.001	0.000
F	0.225	0.203	0.168	0.207	0.210	0.448
Cl	0.001	0.002	0.002	0.002	0.001	0.004
OH	3.770	3.800	3.830	3.790	3.790	3.550
Al ⁽⁴⁾	1.780	1.760	1.780	1.620	1.780	1.700
Al ⁽⁶⁾	3.340	3.420	3.520	3.410	3.500	3.191
Y	3.840	3.860	3.870	3.810	3.880	3.710
A	1.990	1.980	1.960	1.910	1.860	1.880
Mg*	0.004	0.164	0.004	0.007	0.005	0.139
Fe*	0.996	0.836	0.996	0.993	0.995	0.861

Analyses by electron microprobe; cations based on 22 oxygens; n.d.: not detected. Mineral compositions were carried out with a CAMECA SX-100 electron microprobe from the Scientific-Technical Services of the University of Oviedo. This microprobe was operated with an accelerating potential of 15 kV and a sample current of 15 nA, the counting time being 10 s for major elements and 20 s for trace elements (Ba and Rb).

with the metamorphic host rock. They occur in minute anhedral interstitial crystals (Fig. 4).

Cassiterite is the main ore mineral in the Penouta granite and the main Sn mineral. In the granite it exhibits a grain size ranging between 2.2 mm and 30 µm. Larger crystals (up to 3 cm in size) were found in the greisen and quartz veins. In the granite it occurs in association with essential minerals as alkali feldspars, quartz and white micas, but also with beryl, apatite and Nb-Ta oxides. The cassiterite distribution pattern in the granite is complex, with high abundances in the apical zone, but also in intermediate levels. Nevertheless, the highest cassiterite abundance occurs in the greisen. Microprobe analyses of cassiterites in the granite show compositions in Nb₂O₅ (2.22–0.16 wt%), Ta₂O₅ (3.7–0.51 wt%), and FeO (0.94–0.11 wt%, Table 5) that are similar to those of magmatic cassiterites (e.g. Haapala, 1997; Costi et al., 2009).

Nb-Ta oxides are ubiquitous minerals in the granite, but lack in the host rock and quartz veins. In the granite they occur from the bottom to the top of the body as euhedral to subeuhedral crystals with a symmetric, asymmetric or patchy chemical zoning (Fig. 4), the latter being especially common in samples from the upper levels, where columbite crystals are always larger. The crystal rims are usually Ta-enriched relative to the cores, which are Nb-rich. These zoning patterns are the rule in columbite-tantalite-bearing granites (e.g. Helba et al., 1997; Huang et al., 2002). The grain size of columbite-tantalite ranges between 30 and 580 µm. Columbite-tantalites are the most abundant Nb-Ta oxides in the Penouta gran-

ite, whereas microlite (Fig. 4) is scarce and has only been found in the apical zone.

Kaolinite is a secondary mineral phase mainly developed in the weather-exposed leucogranite (up to 50 m thick), decreasing or disappearing when the leucogranite is beneath the metamorphic rock (e.g. strongly mineralised leucogranites from drill holes 3 and 4). The overall kaolinite abundance in the deposit has been estimated to be about 0.3 wt%, whereas in the kaolinite front the abundance is around 20 wt% (estimated by the MINSQ code, Herrmann and Berry, 2002).

6. Geochemistry

6.1. Major element geochemistry

The geochemical classification diagram of Middlemost (1994) reveals that most of samples are alkali feldspar granites, with samples from the western sections plotting onto the granite field, as a consequence of their lower alkali contents (Fig. 5). All the samples show a peraluminous character (A/CNK molar ratio ranging from 1.05 to 1.83) with the lowest values (weakly peraluminous) in the samples from the apical zone, where aluminous minerals, as garnet and white mica, are less abundant. The same peraluminous evolution has been reported in the Nuweibi Ta-bearing leucogranite, where the more peraluminous the magma is, the lower Ta abundance. The moderate K₂O contents (4.07–2.22 wt%) are typical

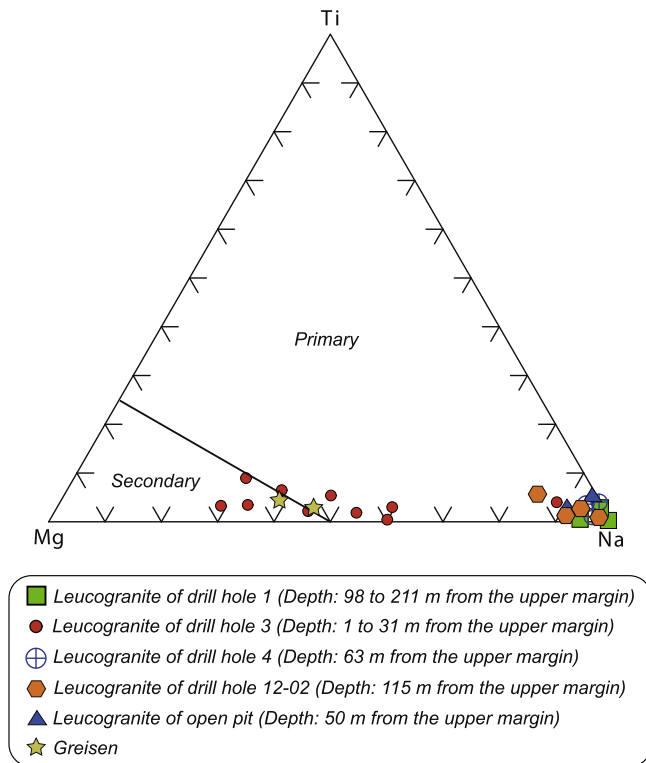


Fig. 3. Classification of white micas in the diagram of Miller et al. (1981).

of magmas of calc-alkaline to high-K calc-alkaline affinities (see Peccerillo and Taylor, 1976). SiO_2 contents range between 77.2 and 70.08 wt%, with the highest abundances in the deepest samples (Fig. 6). Na_2O contents range from 2.5 to near 8, with the high-

est values in the samples from the eastern sections. Al_2O_3 (18.24–14.05 wt%) and Na_2O (7.74–2.6 wt%) increase from the bottom to the top of the granite body. K_2O and $\text{Fe}_2\text{O}_{3\text{t}}$ (1.14–0.27 wt%) are positive correlated relative to SiO_2 (Fig. 6), with the lowest contents in the eastern sections, which can be explained in terms of a higher abundance of ferrous white mica and garnet in the samples of the western section relative to those of the eastern ones. MgO (0.09 wt% to b.d.l.) and TiO_2 (0.01 wt% to b.d.l.) are strikingly low. Phosphorous exhibits a poor correlation with SiO_2 and low contents (<0.07 wt%), with the highest contents in the apical zones. These phosphorous concentrations classify these granites as low-phosphorous granites according to Linnen and Cuney (2005), which are commonly associated with metaluminous I-type and A2-type granites of Eby (1992). The scarcity of apatite and monazite in the Penouta granite justifies these low-P concentrations. Furthermore, very low CaO contents (mostly <0.2) indicate the ubiquitous occurrence of low-Ca plagioclase and the scarcity of apatite.

6.2. Trace element geochemistry

Trace elements controlled by the main minerals, as Sr (68.6–1.08 ppm) are negative correlated relative to SiO_2 (Fig. 7), in a similar fashion to Al and Na, and point to albite strongly controlled Sr variations. Similarly, Rb (1355–527 ppm) and K_2O show the same positive evolutionary trend with SiO_2 , suggesting that minerals with high Rb contents and a high abundance in the western sections, like white mica and potassium alkali feldspar, played an important role in this distribution.

As in other low-P peraluminous Ta-bearing leucogranites (e.g. the Nuweibi leucogranite – Helba et al., 1997 – or the Ponte Segade leucogranite – Canosa et al., 2012), in the Penouta granite accessory and minor minerals strongly controlled HFSE contents, namely Zr, Ta, Sn, Nb, U and REE. In this regard, Gd (15.6–

Table 4
Representative compositions of garnets from the Penouta granite at different depths.

Sample	D06054	D06054	D05547	D05547	D05547	D05545	D05545	D02755	D02755
Location	Core	Rim	Core	Rim	Rim	Core	Rim	Core	Rim
Drill hole	1	1	1	1	1	1	1	3	3
Depth (m)	249	249	135	135	135	129	129	179	179
SiO_2 (wt%)	36.47	36.54	36.46	36.10	35.50	36.43	36.33	36.15	36.01
TiO_2	0.03	n.d.	n.d.	n.d.	0.02	0.01	0.02	n.d.	0.03
Al_2O_3	19.40	19.33	19.41	19.18	19.36	19.68	19.49	19.73	19.27
FeO	23.96	24.24	11.42	11.54	10.67	10.78	11.76	17.92	17.87
MnO	19.97	19.06	32.80	31.47	33.40	32.79	32.35	26.27	26.12
MgO	n.d.	n.d.	n.d.	0.01	n.d.	0.01	n.d.	n.d.	n.d.
CaO	0.29	0.29	0.31	0.92	0.42	0.34	0.50	0.31	0.30
Na_2O	n.d.	0.02	n.d.	0.02	0.04	n.d.	n.d.	0.01	n.d.
Sum	100.12	99.47	100.40	99.24	99.41	100.05	100.45	100.38	99.59
Si apfu	3.02	3.04	3.01	3.01	2.96	3.01	2.99	2.98	3.00
Ti	0.00	–	–	–	0.00	0.00	0.00	–	0.00
Al	1.89	1.90	1.89	1.88	1.90	1.92	1.89	1.92	1.89
Fe^{3+}	0.02	0.02	0.02	0.05	0.02	0.02	0.03	0.02	0.02
Fe^{2+}	1.55	1.58	0.67	0.69	0.60	0.66	0.70	1.14	1.13
Mn	1.40	1.34	2.29	2.22	2.36	2.30	2.26	1.84	1.84
Mg	–	–	–	0.00	–	0.00	–	–	–
Ca	0.03	0.03	0.03	0.08	0.04	0.03	0.04	0.03	0.03
Na	–	0.00	–	0.00	0.01	–	–	0.00	–
<i>End-member molecules (%)</i>									
And	5.37	5.16	5.65	5.86	7.22	4.16	5.71	4.99	5.68
Uva	0.00	0.00	0.00	0.00	0.00	0.00	0.00	0.00	0.00
Gros	0.00	0.00	0.00	0.00	0.00	0.00	0.00	0.00	0.00
Sps	44.86	43.54	72.89	71.88	73.95	74.34	72.03	58.67	58.42
Pyr	0.02	0.00	0.00	0.04	0.00	0.03	0.00	0.00	0.00
Alm	49.75	51.30	21.46	22.23	18.83	21.47	22.26	36.34	35.90

Analyses by electron microprobe; cations based on 8 cations; Fe^{3+} estimated by charge balance; the topographic level of drill hole 1 is 129 m below drill hole 3; n.d.: not detected. Electron microprobe methods as in Table 3.

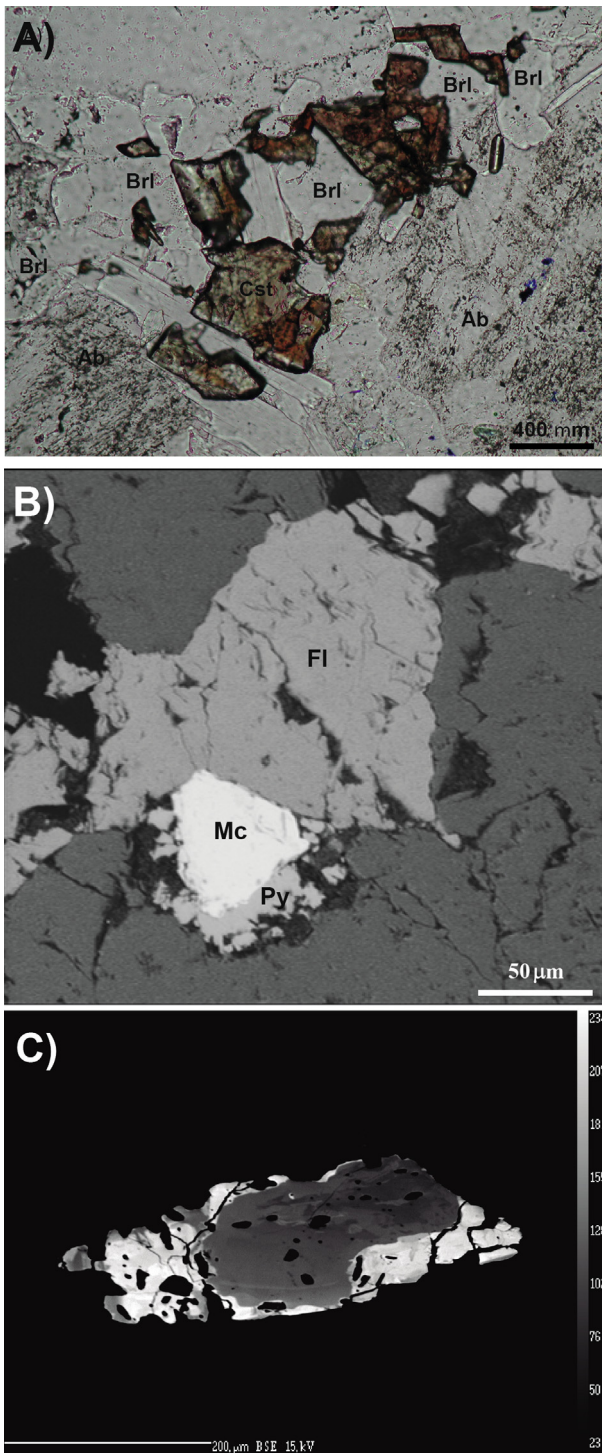


Fig. 4. A) Photomicrograph of cassiterite (Cst) in association with beryl (Brl) in a Sn-enriched sample (drill hole 1). At this level columbite-tantalite occurs almost exclusively as small crystals hosted by cassiterite. B) Back-scattered electron image of fluorite (Fl) and microlite (Mc) in apical samples. C) Back-scattered electron imaging of zoned columbite-tantalite in a apical sample.

0.1 ppm) is likely related to garnet/monazite control, with the lowest contents in samples of the apical zones. Similarly, Y shows depletion from western to eastern section (Fig. 7) and could be related to monazite control. Conversely, elements like Ta (181.5–19.8 ppm), Sn (3340–28 ppm) and, in lesser extent Hf (10.5–4.5 ppm) and Nb (106–37.5 ppm) tend to have a negative correlation with silica (Fig. 7), with the higher contents towards

the apical zones. Ta and Sn trends are the expected result of igneous fractionation, in accordance with Helba et al. (1997). Furthermore, the good positive correlation between Ta/Nb and Na_2O indicates the Ta evolution was concomitant with the albite enrichment of the apical zones.

P and Ta contents of the Penouta granite are similar to those of peraluminous rare-metal granites from the Arabian-Nubian Shield (see compilation of Küster, 2009) and those of low-P and Ta-bearing granites described by Raimbault et al. (1991). According to Linnen and Cuney (2005) low-phosphorous granites are associated with high-K, calc-alkaline metaluminous rocks, rich in Th, REE and Y.

Sn is weaker correlated with silica than Ta, with a tendency to increase in the apical zones, but also high contents were observed in samples of medium levels. U abundance (19.07–2.01 ppm, average 9.07 ppm) is higher than the upper lithosphere Clarke value (av. 2.7 ppm), indicating a “fertile” source of U.

REE chondrite-normalised distribution patterns are very similar in all the samples (Fig. 8), which is a good evidence for a common origin. All the samples show a strong enrichment in MREE (average $\text{Tb}_N/\text{Yb}_N = 66$) and a lack of LREE enrichment relative to MREE (average $\text{La}_N/\text{Sm}_N = 0.26$), although a slight increase of LREE is observed relative to HREE (average $\text{La}_N/\text{Yb}_N = 10.9$), as well as a marked Eu negative anomaly (average $\text{Eu}/\text{Eu}^* = 12.1$). It is noteworthy that western sections show higher abundances in Gd, Tb, Sm as well as LREE and ΣREE (Fig. 8), defining a M-type of REE, probably in line with the above mentioned strong control of garnet and Gd-enriched monazite in the REE distribution. The low HREE contents of most samples indicate a limited effect of garnet and zircon (minerals that highly fractionate these elements, see Rollinson, 1993) in controlling HREE patterns. Similarly, the low-P contents also justify the limited role played by apatite in the REE distribution. The Eu anomalies and the distribution in Gd, Tb and Sm closely resemble those of albite granites, as the Yichun topaz-lepidolite leucogranite (Huang et al., 2002). The convex-upward segment of the REE patterns for Sm and from Gd to Dy is an expression of the lanthanide tetrad effect in the 2 and 3 tetrads, with values ranging between 1.7 and 2.1 (Table 1).

6.3. Vertical variations in whole-rock chemistry of selected drill holes

The chemical variations of the selected constituents were depicted with respect to height (Fig. 9). Ta contents generally increase upward indicating the incompatible character of this element from bottom to top of the body, frequently with a higher Ta enrichment at the upper level (Fig. 9). Nb also exhibits an incompatible behaviour from bottom to top, but with a compositional range more restricted relative to Ta. Sn shows a progressive enrichment in the eastern and central sections, with a more pronounced enrichment in the upper margin (Fig. 9), in contrast to the western profile, where the highest Sn contents are in the medium zones.

In contrast to ore element distribution with height, REE exhibit a progressive decrease upward (see Fig. 9 for Gd evolution), suggesting their compatible behaviour in the melt.

Finally, the Zr/Hf ratio generally has a tendency to depletion in the apical margin, where the Hf abundance is higher than Zr. Zr/Hf ratio is commonly lower than 4, in a similar fashion to highly fractionated rare-metal granites, as those of Orlovka and Egypt described by Melcher et al. (2016).

7. Geothermometric constraints

To constrain differences in liquidus temperature (maximum temperature at which crystals can co-exist with the melt in thermodynamic equilibrium) from bottom to top of the body the satu-

Table 5
Representative compositions of cassiterites from the Penouta granite.

Sample	Samples of section 3				Samples of section 1 with high Sn contents				
	2662 C6	2666B C1	2722 C2	2724 C1	5545 C1	5545 C2	5547 C1	5547 C2	5547 C2
TiO ₂	0.12	0.01	n.d.	n.d.	0.01	n.d.	n.d.	n.d.	n.d.
Al ₂ O ₃	0.03	0.03	0.04	0.01	0.02	0.02	n.d.	0.02	0.02
FeO	0.28	0.94	0.21	0.11	0.68	0.85	0.48	0.81	0.57
MnO	0.02	0.12	0.07	0.08	n.d.	0.13	0.11	0.12	0.09
Nb ₂ O ₅	0.16	2.22	0.36	0.18	1.17	1.00	1.31	1.17	1.51
Ta ₂ O ₅	1.70	3.20	1.94	1.27	1.05	3.70	0.51	3.07	0.85
SnO ₂	98.49	94.80	98.31	100.30	97.78	94.77	97.24	95.58	97.85
Sum	100.79	101.31	100.93	101.94	100.71	100.47	99.65	100.77	100.89
Ti apfu	0.00	0.00	–	–	0.00	–	–	–	–
Al	0.00	0.00	0.00	0.00	0.00	0.00	–	0.00	0.00
Fe	0.01	0.02	0.00	0.00	0.01	0.02	0.01	0.02	0.01
Mn	0.00	0.00	0.00	0.00	–	0.00	0.00	0.00	0.00
Nb	0.00	0.02	0.00	0.00	0.01	0.01	0.01	0.01	0.02
Ta	0.01	0.02	0.01	0.01	0.01	0.03	0.00	0.02	0.01
Sn	0.98	0.93	0.97	0.98	0.97	0.94	0.97	0.95	0.96
Sum	1.00	1.00	1.00	1.00	1.00	1.00	1.00	1.00	1.00

Analyses by electron microprobe; total Fe as FeO; cations based on 2 oxygens; n.d.: not detected. Electron microprobe methods as in Table 3.

Table 6
Selected mineral compositions used in multi-stage major element-based least-squares modelling and trace element partition coefficients used in Rayleigh/equilibrium crystal-melt fractionation.

Mineral	Kfs	Pl	Q	Mus	Grt 1	Grt 2
SiO ₂	64.7	68.6	100	46.1	36.1	36.3
TiO ₂	–	0.01	–	–	–	–
Al ₂ O ₃	18.0	19.2	–	33.9	19.2	19.3
FeO	–	–	–	3.41	11.5	23.9
MnO	–	0.02	–	0.15	31.5	20.0
MgO	–	0.01	–	–	0.01	–
CaO	–	0.19	–	0.01	0.92	0.25
Na ₂ O	0.29	11.2	–	0.39	0.02	0.02
K ₂ O	15.8	0.13	–	10.7	0.01	–
X _{Fe}	–	–	–	0.99	0.22	0.50
X _{An}	0.00	0.01	–	–	0.00	–
X _{Or/Mus}	0.97	0.01	–	0.98	–	–
Kd _{Nb}	0.03	–	0.00001	3.5	0.07	0.07
Kd _{Ta}	0.03	–	0.00001	0.4	0.12	0.12

Partition coefficients were taken from the compilations of EarthRef.org: GERM Partition Coefficient Database and references therein, except for muscovite that was taken from Raimbault and Burnol (1998); mineral abbreviations after Kretz (1983); –: below detection limit, not calculated or not available.

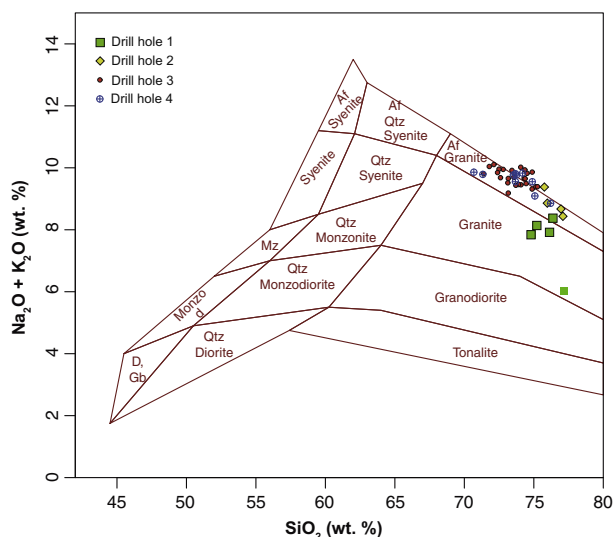


Fig. 5. Na₂O + K₂O vs. SiO₂ classification diagram of plutonic rocks according to Middlemost (1994). The diagram was carried out using the GCDkit package (Janoušek et al., 2006).

ration model of the melt with respect to trace elements (e.g., Zr and LREE, see Watson and Harrison, 1983; Montel, 1993) that are strongly enriched in accessory minerals, as zircon and monazite, were used. The depletion in REE and Zr/Hf from bottom to top supports zircon and monazite were saturated mineral phases (e.g. Hoskin et al., 2000). Samples from the lower part of the granite yielded the highest values (around 665 °C), whereas values between 580 and 610 °C were obtained in the apical zone (Table 1). Very similar temperature estimates were derived from both geothermometric applications (Table 1), suggesting a limited role played by Hf in zircon solubility. Moreover, Ti-in-zircon thermometry was also carried out (Watson et al., 2006) but the results were inconsistent (837 °C on average and temperatures up to 1053 °C for an activity of TiO₂ = 0.7; not shown). Low calculated liquidus temperatures obtained by monazite and zircon saturation modelling have only been obtained experimentally in granite systems with fluxing elements (e.g. F, see Manning, 1981; Xiao-Lin et al., 1999). According to experimental approaches on granite melts with fluxing elements (Manning, 1981; Xiao-Lin et al., 1999) and melting data of glass inclusions from ongonites reported by Naumov et al. (1971) the solidus temperatures (point at which the melt completely crystallises) in this kind of melts are particularly low and they could be lower than 550 °C.

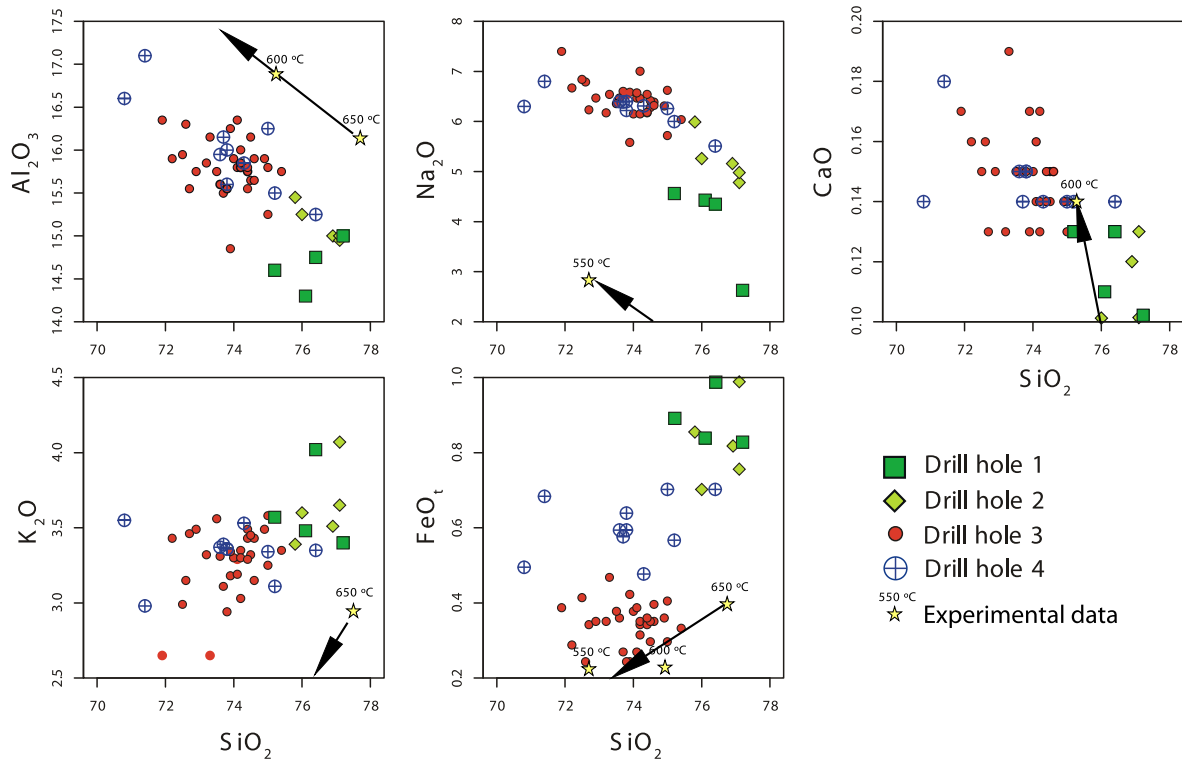


Fig. 6. Harker diagrams for major elements. The composition of experimental melts in the albite granite-H₂O-HF system at different temperatures and for an initial fluorine content of 2 wt% are also included (data from Xiao-Lin et al., 1999).

The phengite barometer (Massonne and Schreyer, 1987; Massonne and Chopin, 1989) indicates emplacement around 300 MPa.

8. Discussion

8.1. Subhorizontal emplacement of a single magma pulse

From the previous sections, evident evolutionary trends in Gd, Zr, Ta, FeO, Na₂O with SiO₂ have been revealed involving samples from all the sections (Figs. 6 and 7). Since the upper samples of the eastern sections are at a higher topographic level, this difference in the topography could easily explain the occurrence of a cupola zone in the eastern sections and a deeper level in the western drill holes.

Considering the same topographic level in two separate drill cores (1 and 3), a comparison of the concentration of elements correlated with silica (e.g. REE, Ta and the Zr/Hf ratio) reveals quite similar compositions in both sections for the selected topographic level (Fig. 10). The latter supports the higher abundance in Ta and the lower concentrations in REE and Zr in eastern sections could be explained in terms of their higher topographic levels relative to the western ones, with the cupola zone being located to the East. This topographic factor as key to explain contrasted geochemical variations among western and eastern samples is in line with a single magma pulse instead of an intrusive juxtaposition of two or more batches of differently-evolved magmas, as it is the case of other Ta-bearing albite granites (e.g. the Nuweibi granite, see Helba et al., 1997; the Bouvair granite, see Cuney et al., 1992). Additionally, in the light of the invariable composition observed with the height in the two distant drill cores studied, a subhorizontal magma emplacement and a subsequent flattened shape of the granite body can be inferred.

8.2. Differentiation process from bottom to top of the granite body

a) Whole-rock geochemistry constraints: variation diagrams

The melt in the Penouta granite was probably emplaced as a single magma batch instead of successive magma batches more evolved upward without any stage of replenishment, as it is deduced by the absence of gaps in the variation diagrams, the continuity in REE patterns and in diagrams showing composition with respect to height (Figs. 6–8). The absence of switch from incompatible to compatible behaviour (bell-shaped trends) has not been observed in bivariate diagrams or diagrams with height, suggesting that any mineral phase reached the saturation from the emplacement to the solidification stage. In contrast to the evolution of biotite or two mica granites, where silica increases and Fe depletes with the evolution (e.g. López-Moro et al., 2012), in the albite granite of Penouta the highest contents in Fe are shown by the richest Si samples. This behaviour has also been described in experimental works in the albite granite-H₂O-HF system (Xiao-Lin et al., 1999), where a concomitant enrichment in Al, Na and Ca occurs as the temperature decreases (see Fig. 6), supporting that the less evolved samples and probably the initial magma are in the lower margin of the Penouta granite. Experiments also confirm depletion in K₂O with SiO₂ as temperature decreases (Fig. 6). The variations in these elements together with the Rb depletion (Fig. 7) from the least to the most evolved samples points to muscovite, alkali feldspar, garnet and quartz strongly controlled these elements. Conversely, the increase of Sr, Al₂O₃, CaO and Na₂O from the least differentiated to more evolved samples suggest albite accumulation or a change in the ternary cotectic due to a fluorine enrichment (Manning, 1982) and thus consistent with a modelling whereby fluorine increased upwards. Similarly, REE, Y and Zr decrease

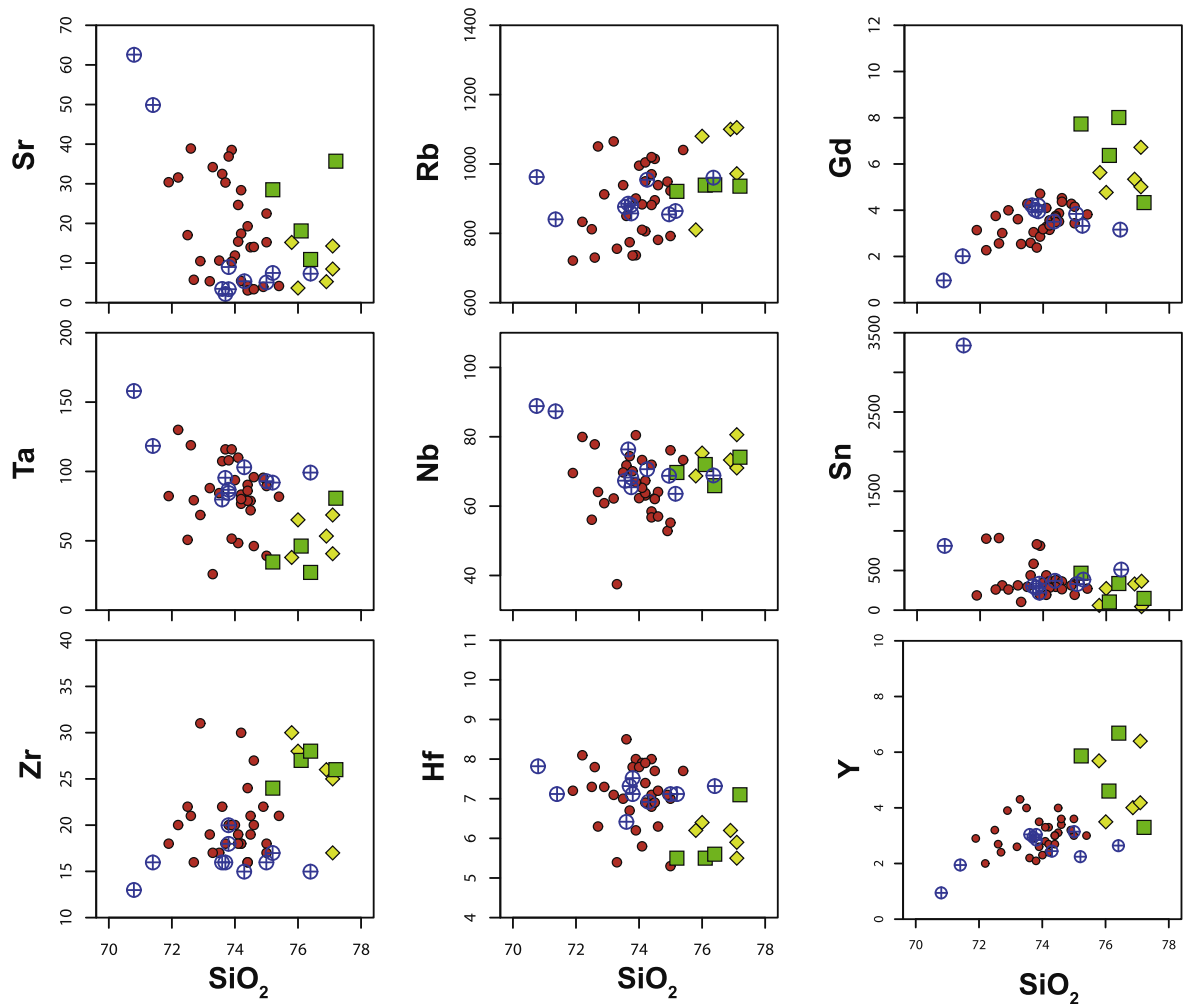


Fig. 7. Variation diagrams for selected trace elements. Symbols as in Fig. 6.

concomitant with silica, pointing to monazite, garnet and zircon were saturated, liquidus and fractionated phases that would have strongly controlled the variations of these elements in the residual liquid.

b) Whole-rock geochemistry constraints: least-squares mass-balance modelling

To check the evolution of the melt from bottom to top and the assumption of a parental magma in depth with successive daughters deriving upwards, major element least-square modelling was performed with the OPTIMASBA code (Cabero et al., 2012). The chosen starting melt was the least evolved sample of the western section (deepest samples) and several more evolved samples from eastern sections as daughters. Additionally, a model involving the deepest sample of eastern drill hole and the more evolved sample of the same drill hole was also carried out (Fig. 11). In all models quartz, alkali feldspar, garnet, muscovite and albite were selected, by default, as mineral phases involved in the process, but the best matches were always obtained excluding albite as removed or added mineral, which is also in line with the enrichment of Na, Al and Ca with the evolution observed in variation diagrams (Fig. 6). The model justifies that the selected residual liquids are genetically related to the assumed initial magma; otherwise, the sum of the squares of the residuals would be higher, i.e. the match would be worse. Similarly, the model is consistent with an

evolution from bottom to top of the body, since the proportion of the residual liquid decreases upward (compare model 1 and 3 in Fig. 11). The estimated residual liquid from the least to the most evolved daughter (64% in model 3, or 60% considering model 1 and 2 in Fig. 11) is also not dissimilar to the proportion of the remaining melt in melting experiments (50% considering a starting point with a 2% of fluorine, Xiao-Lin et al., 1999) at 600 °C, the latter being the average temperature of zircon and monazite for the selected daughter.

c) Mineral-chemistry constraints on the gangue minerals

Some mineral phases of the Penouta granite exhibit chemical variations from bottom to top, which could be the result of the evolution of the melt. The evolution upwards of almandine depletion joined to the increase in spessartite molecule of garnets of the Penouta granite have been reported in garnets of zoned pegmatite fields, representing a progressive degree of fractionation (e.g., Baldwin and von Knorring, 1983; Müller et al., 2012). However, whole-rock Fe and Mn variations could not only be controlled by garnet, but also by muscovite. Partition coefficient values of muscovite for Fe and Mn ($D_{Fe}^{Mu-melt} = 8$; $D_{Mn}^{Mu-melt} = 2$; Raimbault and Burnol, 1998) indicate that the melt may become strongly depleted in Fe relative to Mn as a consequence of muscovite crystallisation, which is in line with the lower iron contents of apical muscovites from the Penouta granite

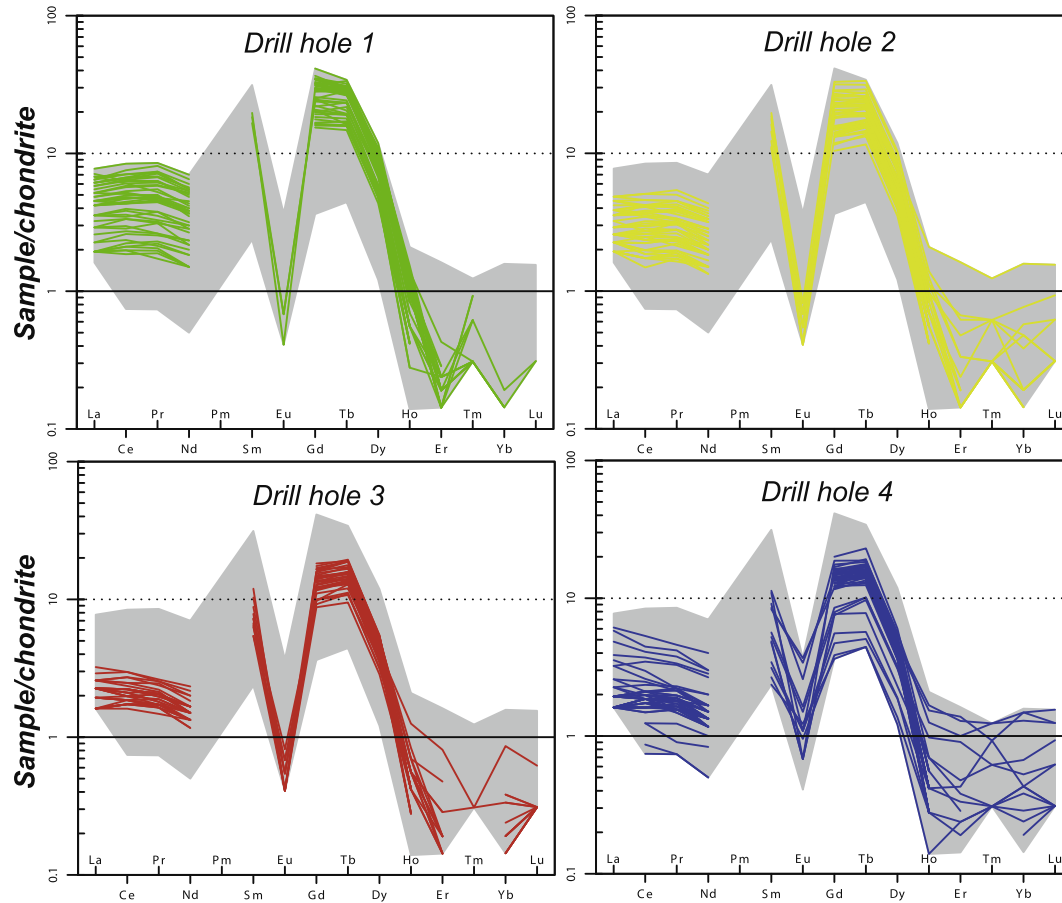


Fig. 8. Chondrite-normalised REE contents of drill holes from the Penouta granite. Normalised values after Boynton (1984). Shaded field: complete range of data.

(Table 3). Similarly, chemical variations of garnet and muscovite support the notion that the higher mineral abundances of these minerals in depth (Table 2) are mainly due to crystal-melt evolution instead of accumulation processes. Moreover, monazites of the Penouta granite have lower LREE contents upwards (Table 2A). LREE are essential constituents in this mineral and its fractionation may prompt their progressive impoverishment, as it has been reported in the Yichun high-P albite granite (Huang et al., 2002). A binary mixing modelling involving monazite added (0.003 wt%) to an evolved sample from the apical zone reproduces very well the LREE contents of a sample from the bottom of the granite (Fig. 12), pointing to monazite strongly controls LREE signature in the melt. However, unlike what happens in whole-rock geochemistry, Gd and Y increase in monazite upwards (Table 2A), suggesting that these elements were partitioned by garnet. The progressive decrease of garnet proportion upwards probably led to an accommodation of available Gd and Y in monazite in a bigger extent that it occurred in deeper zones. The latter is also confirmed by the mixing modelling performed, as Gd, Tb and Dy are not matched very well (Fig. 12), suggesting that other minerals fractionating HREE played an important role in the distribution of these element (e.g., garnet and zircon).

A similar scenario occurs with zircon, as the observed rise of Hf budget in zircon upwards can be satisfactorily explained by the fractionation of zircon itself, which causes a higher depletion in Zr relative to Hf in the melt (Linnen and Keppler, 2002; Claiborne et al., 2006; Rubatto and Hermann, 2007).

Apatite tends to have higher fluorine content in the apical zone of the granite. This fluorine enrichment could indicate: (i) an enrichment upwards in the fluorine content of the melt, due to crystal fractionation of phases without or with low fluorine contents, or (ii) a depletion in the apical zone of minerals containing fluorine (e.g. white mica), as a consequence of crystal-melt fractionation processes.

Hence, mineral-chemistry, crystallisation-melting experiments and the results of the major element least-square modelling allow to constrain the evolution of the melt in the Penouta granite, with a decrease in quartz-alkali feldspar-muscovite-garnet \pm zircon \pm monazite from bottom to top. A point worthy of mention is that the evolution of the melt in the Penouta granite (e.g. depletion of silica with the evolution) is contrary to that of less evolved granite melts (e.g., biotite and two mica granites), probably by the higher contents of fluxing elements, as fluorine, in the Penouta granite melt (see Manning, 1981).

8.3. Ore-element evolution

a) Saturation of ore minerals

Continuous trends of Ta and Sn with height are the rule in the Penouta granite, representing evidence of the saturation of tantalite and cassiterite were not attained, otherwise a depletion in Ta, Nb and Sn would be observed once columbite-tantalite and cassiterite reached their saturation (Evans and Hanson, 1993; Hoskin et al., 2000). This assumption is in agreement with the experimental approaches of manganotantalite-manganocolumbite and cassiterite satu-

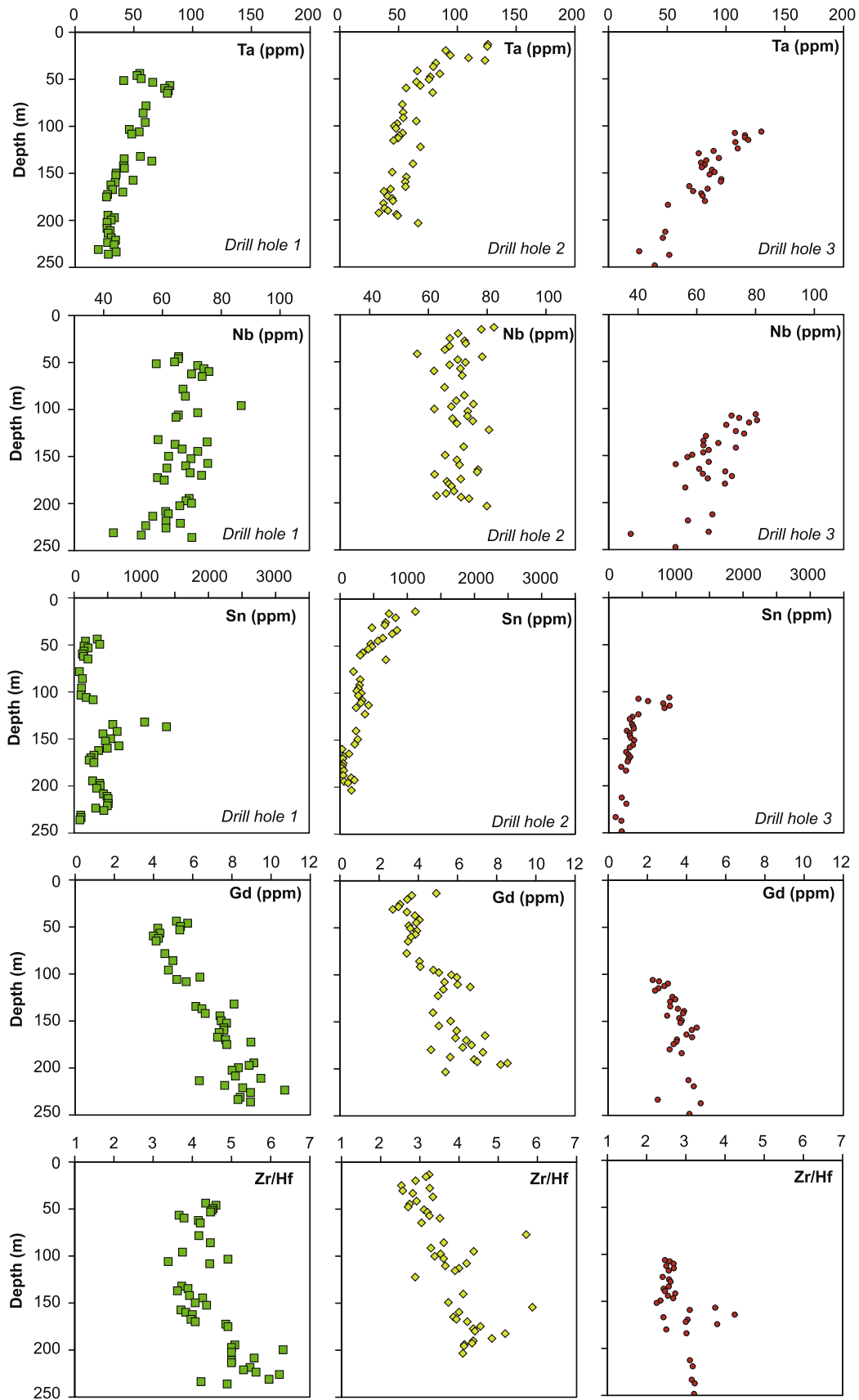


Fig. 9. Chemical variations with height for selected elements in the Penouta granite. Variations of the overlain metamorphic rock were omitted.

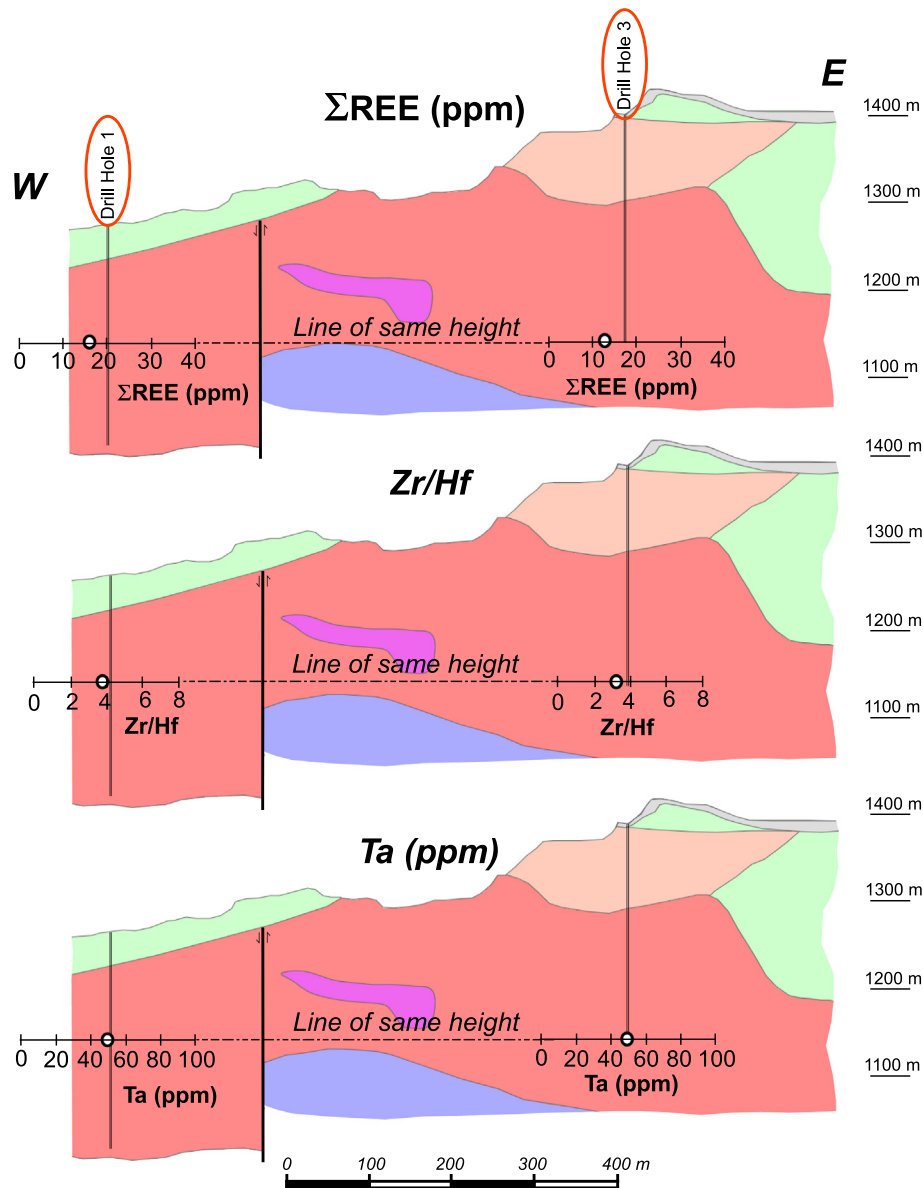


Fig. 10. Topographic effect in geochemical contents of selected elements for the Penouta granite.

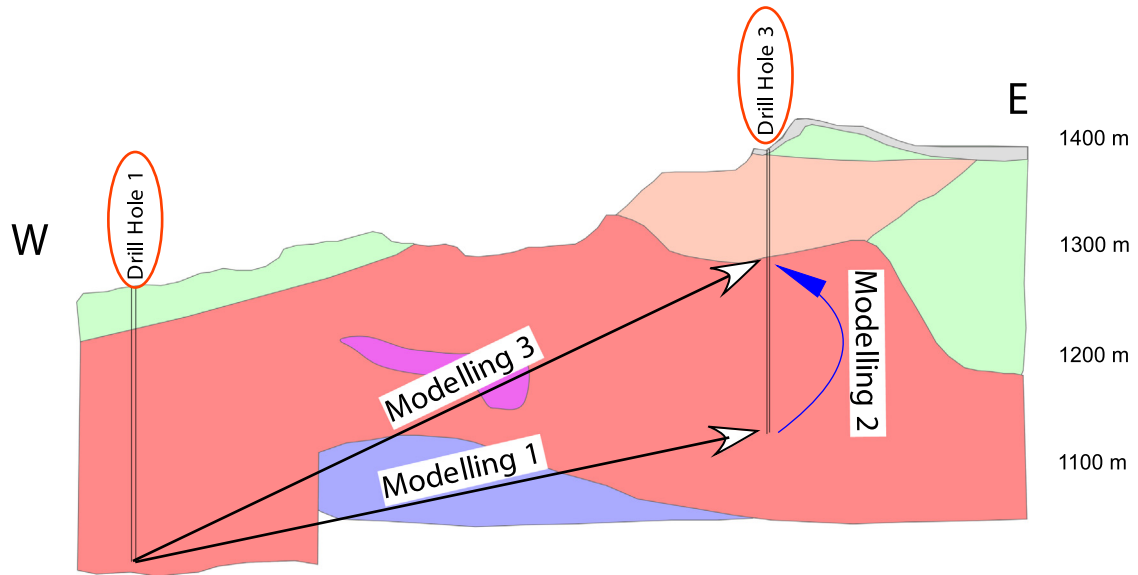
ration (Linnen, 1998; Bartels et al., 2010; Taylor and Wall, 1992; Štemprok, 1990; Bhalla et al., 2005). For instance, by considering a crystallisation temperature of 600 °C for the most evolved sample, the saturation of tantalite would be reached at 649 ppm and 2052 ppm of Ta for a system without and with fluxing elements, respectively; whereas the saturation of cassiterite would occur at 1400 ppm and 849 ppm of SnO_2 in the melt with and without fluxing elements, respectively. These values are higher than the budget of Ta in the Penouta granite, especially when there are also evidences that support the notion of fluxing elements in the melt that would increase the solubility of Ta in the melt. These results are also in line with measured melt inclusions of pegmatites, where Ta concentrations exceed economic Ta deposits in some orders of magnitude (see Thomas et al., 2011).

The occurrence of columbite-tantalite and cassiterite throughout the Penouta granite body in a melt undersaturated for Sn, Nb and Ta could be explained by the existence of a localised saturation and crystallisation adjacent to

growing rock-forming minerals within trapped intercumulus melt (Bacon, 1989; Hoskin et al., 2000), as it has been stated for zircon saturation in granodiorites (Hoskin et al., 2000). Columbite-tantalite and cassiterite would have been formed within non-equilibrium concentration gradients that could explain the often-complex zoning patterns observed in these minerals, regardless of the level where they appear.

b) Concentration of Ta and Nb and the evolution of Ta/Nb in the melt

The lack of saturation of Nb-Ta oxides in the Penouta albite granite points to normal zoning observed in these minerals, consisting of Nb-rich cores and Ta-rich rims, is not the reason to explain an increase in Ta and in the Ta/Nb ratio in the melt, via crystal fractionation of Nb-Ta oxides, as it has been proposed in pegmatites (Chevychev et al., 2010; Černý et al., 2012) or in leucogranites (Linnen and Cuney, 2005). Similarly, a dependence of alumina saturation index with the Ta/Nb ratio or Ta solubility reported in pegmatite melts (e.g. van Lichtervelde et al., 2010) should also be discarded in the Penouta granite, as both parameters are



Multi-stage major element-based least-squares modelling

Modelling	Fractionating assemblage				SSE	F (wt.%)
	Kfs	Grt	Mus	Q		
Modelling 1						
Lower part drill hole 1 (P06053)	3.9	1.8	4.7	13.6	0.001	76
↓						
Lower part drill hole 3 (P02944)	<i>16.3</i>	<i>7.5</i>	<i>19.5</i>	<i>56.7</i>		
Modelling 2						
Lower part drill hole 3 (P02944)	1.6	0.3	3.5	10.6	0.0001	84
↓						
Upper margin granite DH 3 (P02666)	<i>9.9</i>	<i>1.8</i>	<i>22.1</i>	<i>66</i>		
Modelling 3						
Lower part drill hole 1 (P06053)	4.8	1.8	7.7	21.6	0.001	64
↓						
Upper margin granite DH 3 (P02660)	<i>13.5</i>	<i>5.1</i>	<i>21.4</i>	<i>60</i>		

SSE: Sum of squared residuals; F: percentage of residual liquid; mineral abbreviations after Kretz (1983); numbers in brackets are the names of samples used in modelling; numbers in italics: cumulate minerals normalised to 100; MnO, P₂O₅ and TiO₂ not considered in modelling.

Fig. 11. Schematic diagram showing the least-squares mass balance modelling performed for the Penouta granite. The modelling was carried out assuming the deepest sample of the drill core 1 (D06053) represents the initial/parental magma. Samples from the eastern drill hole 3 at different topographic levels (samples D02944 and D02666), including the apical zone, were considered as residual liquids. The composition of fractionated minerals is compiled in Table 6. Note the excellent match of modelling exemplified by the sum of squares due to error (SSE).

negatively correlated (Fig. 13). Alternatively, two possibilities could explain the Ta, Nb and Ta/Nb ratio variations observed:

- (i) An increase in fluorine content could have progressively increased upward the solubility of Ta relative to Nb (Linnen, 1998; Bartels et al., 2010), favouring the crystallisation of Nb-Ta oxides within a trapped inter cumulus melt with higher Ta/Nb ratio

upwards. Fluorine enrichment upwards seems likely in the Penouta granite by the occurrence of fluorite only restricted to the apical zone of the granite. However, recently, a higher solubility of Ta and Nb in relation with fluorine in the melt has been questioned in solubility experiments of manganotantalite and manganocolumbite (Fiege et al., 2011; Aseri et al., 2015).

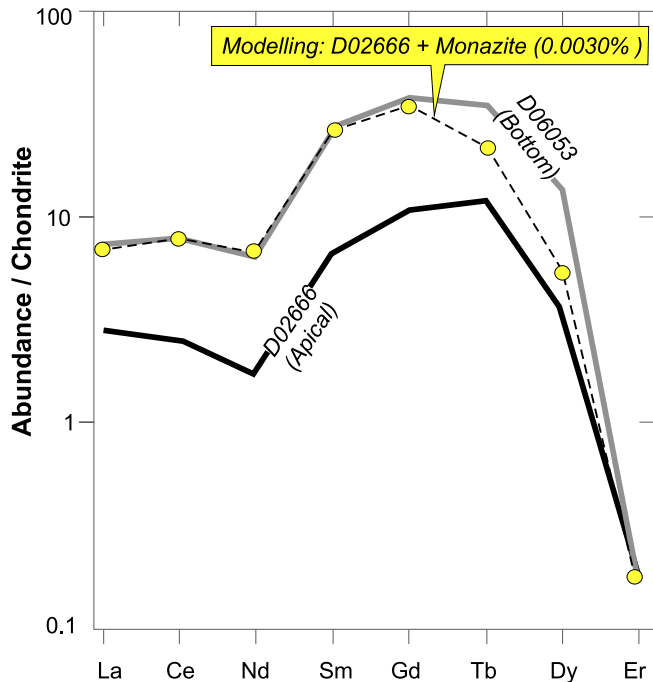


Fig. 12. Chondrite-normalised REE patterns (values from Boynton (1984)) showing samples from the upper (D02666) and lower (D06053) parts of the leucogranite and a mixing model, where monazite of the Penouta leucogranite was added to the most evolved sample of the albite leucogranite (D02666). Equations of two mixing components after López-Ruiz and Cebriá (1990).

(ii) The existence of a fractionated mineral phase removing Nb in higher extent than Ta from the melt. Muscovite, biotite and amphibole have been implicated as minerals able to fractionate Ta from Nb in granite melts (Raimbault and Burnol, 1998; Stepanov et al., 2014). Biotite and amphibole are missing in the Penouta granite, but white mica is an essential primary mineral (Fig. 3) and its fractionation could have had a clear effect on the evolution of the melt. Crystal fractionation modelling considering modes and minerals obtained via least-squares mass-balance modelling (Fig. 11) is in a close match with the wide set of data from the Penouta granite (Fig. 13). Hence, Ta and Nb variations could be properly explained by a fractionation process occurring from bottom to top that includes white mica, quartz, alkali feldspar and garnet as main fractionated mineral phases, but excludes columbite and tantalite. According to this proposal, and in line with previous reasoning, columbite and tantalite would be the result of localised saturation within a trapped intercumulus melt. This modelling would explain the more pronounced enrichment in Ta with height than that of the Nb (Fig. 9) in terms of a higher bulk distribution coefficient of the fractionating assemblage in Nb ($D_{Nb} = 0.59$) than in Ta ($D_{Ta} = 0.08$). Similarly, the observed relationship between Ta and Ta/Nb with A/CNK (Fig. 13) may be compatible with the crystal fractionation process, as the removal of minerals with high alumina saturation index, like muscovite, garnet and in lesser extent alkali feldspar, justifies the progressive depletion in the A/CNK from bottom to top of the body. Moreover, the close match of the modelling in the Ta/Nb-Ta diagram is in agreement with a limited modification of the Ta/Nb ratio by subsolidus fluids.

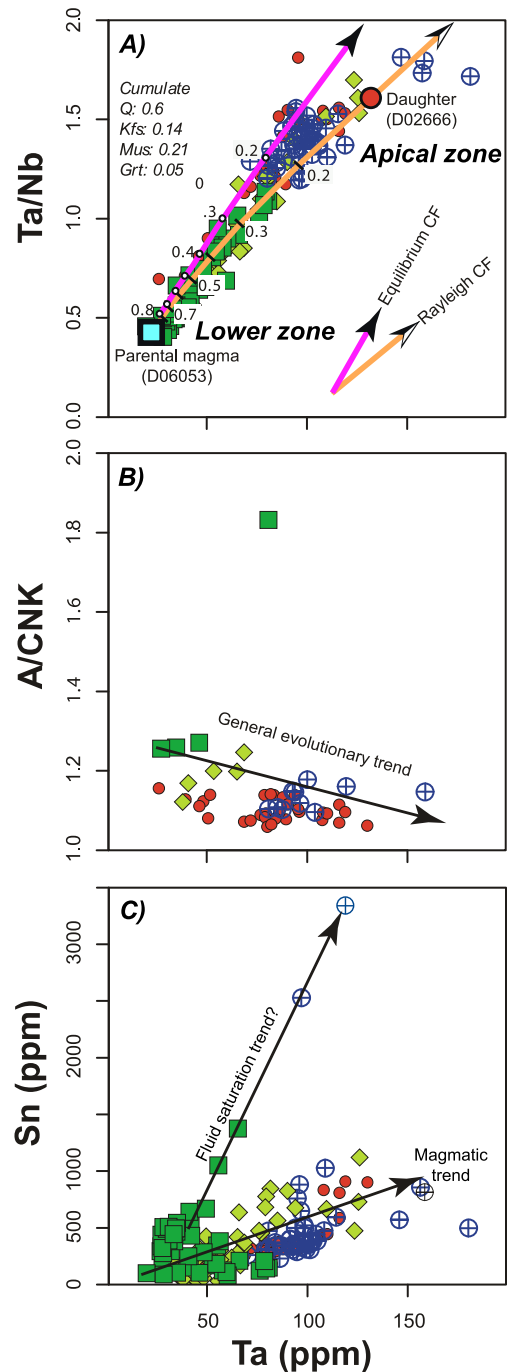


Fig. 13. A) Fractional crystallisation modelling (Rayleigh and equilibrium) for Ta and Nb variations. The modelling was carried out using the mode estimated by the least-squares mass balance modelling (inset in diagram). Partition coefficients compiled in Table 6. Small circles and ticks represent the fractions of residual liquids. B) A/CNK vs. Ta diagram. C) Sn-Ta variation diagram showing a general evolutionary trend owing to fractional crystallisation and a second trend assumed to be consequence of degassing.

c) Sn enrichment at mid-levels: a case of degassing processes? The Sn distribution pattern in the Penouta granite with height commonly shows a progressive enrichment from bottom to top (Fig. 9). Nevertheless, several drill holes exhibit in mid-levels a strong Sn enrichment (e.g. Fig. 9, drill hole 1), where only a concomitant weak increase in the Ta abundance occurs. Therefore, the Sn-Ta distribution pattern at mid levels is clearly different to the most common Sn-Ta

evolutionary trend, which is assumed to be magmatic in origin and in relation to the main differentiation process (Fig. 13). The Sn enrichment of mid-levels could be compatible with a change in the fO_2 conditions in the melt, whose depletion could have led to a higher solubility of SnO_2 in the melt (Linnen et al., 1995), but not in the Ta. However, depletion in the fO_2 should be probably related to assimilation processes at this level, which is not the case according to drill holes studied; besides, a change in fO_2 would not explain the mineral association beryl-cassiterite observed in the most Sn-enriched samples (Fig. 4). It seems likely that Sn contents out the magmatic trends are not linked to fractional crystallisation, but to a fluid phase, as Sn partitions in favour of the fluid and Ta has affinity for the melt (e.g. Linnen and Cuney, 2005). Moreover, the signature of cassiterites in zones of strong Sn enrichment in the granite (Table 5) is typically magmatic in terms of Nb and Ta contents (e.g., Haapala, 1997; Costi et al., 2009). Hence, in the light of the above it follows that an externally derived subsolidus-hydrothermal fluid can be ruled out in explaining the origin of these cassiterites and a magmatic-derived fluid begins to gain strength. This magmatic fluid might be generated by volatile release, process that can be evidenced in the Penouta granite by the occurrence of flat-lying sheets of aplo-pegmatite in the apical zone. A process able to saturate a melt in vapour is depressurisation (e.g. Winter, 2001). This mechanism might be plausible in the Penouta granite taking into account the lower pressure of emplacement, the lower solidus estimates and the strong volatile enrichment of this kind of melts (e.g. Lehmann, 1994). Besides, the occurrence of phenocrysts of quartz, alkali feldspar, albite and white mica hosted in a groundmass composed of the same minerals might indicate a rapid ascent of a crystal mush from a reservoir (magma chamber?) up to the emplacement place (similarly to subvolcanic rocks), thus evidencing a depressurization process in the melt of the Penouta granite. The rapid rise of the crystal mush might be in coherence with the low viscosity of a fluorine-enriched melt (Dingwell et al., 1985).

Another mechanism yielding fluid saturation in a melt is the second boiling, which is induced by crystallisation of anhydrous minerals (as it seems to be occurring in the Penouta granite, Fig. 11) in a cooling scenario. This process has been studied in tabular-like bodies with a similar thickness than the Penouta granite (Boudreau and Simon, 2007) revealing that a crystallising and cooling tabular body develops two separate vapour-saturated zones, namely, at the lower and upper margins. In the upper fluid-saturated zone, fluid exsolved forms pegmatoids, whereas in the lower margin fluid exsolved migrates upward into hotter silicate liquid up to the central part of the body, where it can be resorbed. This modelling predicts well some features of the Penouta granite: (i) flat-lying sheets of aplo-pegmatite occur in the apical zone of the granite body, that joined to the greisen developed in the wall rock might be consequence of upper-margin fluid saturation, and (ii) the absence of pegmatoids in the lower margin, together with a dramatic enrichment in elements with a high affinity by fluids, as Sn and Be, in the medium levels of the Penouta granite could be consistent with a fluid saturation from the lower margin and its resorption in the hotter silicate liquid in the central part (Fig. 14).

According to this modelling, the heat loss in both margins is a key point for the development of a crystallisation-induced degassing (second boiling), that in the Penouta granite might be favoured by its late-orogenic character and the geometry of the granite body. Regarding the former, the Penouta granite was emplaced in a metamorphic pile in the greenschist facies, according to the P-T conditions of the area in the M_3 metamorphic stage (Díez Montes, 2007), that facilitated cooling. Similarly, the Penouta granite is a laminar/laccolith body that exhibits higher contact surfaces with the country rock than a typical stock body for the same amount of melt (López-Moro et al., 2012). This fact might facilitate the rapid cooling and consequently the second boiling and the Sn mobilization in fluid/vapour.

Moreover, vapour separated could also be a contributory factor to trigger, at least in part, the subsolidus overprinting

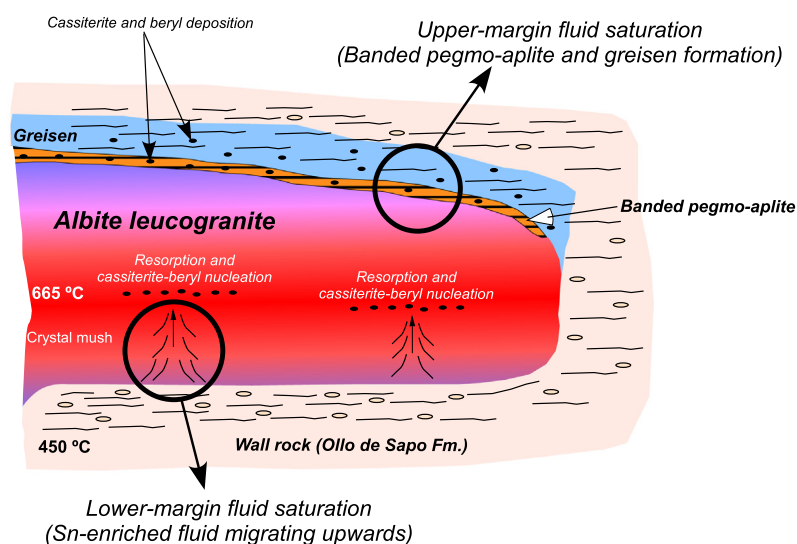


Fig. 14. Interpretative scheme to explain Sn enrichment in medium zones of the Penouta granite by lower-margin degassing. In this modelling a vapour separating from the lower margin transports abundant Sn and Be that are resorbed by the hotter silicate melt at mid-levels of the granite body, thus favouring the nucleation of cassiterite and beryl.

processes affecting the Penouta granite, exemplified, for instance, by the occurrence of mesoperthites or patchy zoning in Ta-Nb oxides.

9. Conclusions

The low viscosity of granite melts with fluxed elements, such as F, seems to be a crucial issue in controlling the lenticular shape and the lateral extension of this kind of melts, as is the case of the Penouta granite. The evolution of these melts in the emplacement place can become quite simple, as it occurs in the Penouta granite, with a single magma pulse laterally extended, with a differentiation process where the melt evolves upwards. The latter is in accordance with mineral chemistry, whole-rock geochemistry, mass balance modelling, Rayleigh fractionation modelling and experimental works. Our results support that Nb-Ta oxides and probably cassiterite were not saturated mineral phases, and it could be the rule in other albite granites. Hence, Nb-Ta oxides would have not fractionated Nb relative to Ta and these mineral phases would have crystallised within the intercumulus trapped liquid at very limited portions of melt. In the light of recent experiments and/or our results, the role played by fluorine in tantalum concentration in the melt is unclear, and the same is true for the peraluminosity of the melt and hydrothermal fluids. The process that best reproduces the Ta and Nb variations in the Penouta granite is fractional crystallisation, including muscovite as fractionated mineral phase. Muscovite fractionation in the Penouta granite can be highlighted by mass balance and trace element modelling performed in this work, mineral chemistry and modal-proportion variations of muscovite observed from bottom to top of the granite body and its predominant primary character. Similarly, crystallisation-melting experiments and the occurrence of white mica phenocrysts in volcanic equivalents to albite granites (ongonites) point to muscovite is a liquidus phase in this kind of magmas. However, further experimental works would be necessary to constrain about muscovite crystallisation in granite systems with a garnet-bearing albite leucogranite as starting point (not only topaz-bearing leucogranites), especially because garnet is a very frequent accessory in rare-metal albite granites (e.g., Penouta, Nuweibi and Abu Dabab). Nevertheless, despite the contribution of fluorine in concentrating tantalum relative to Nb is questionable, the role played by fluorine in decreasing the solidus and the viscosity of the melt protracts crystal fractionation, and enhances crystal settling processes, which both favoured the enrichment in incompatible elements like Ta, Nb and Sn from bottom to top.

The process of Sn concentration in this kind of melts is complicated to be unravelled by the affinity for fluids of Sn and the complexity of carrying out experiments with this element. Bivariate diagrams applied to the Penouta granite resulted to be useful tools to discriminate two contrasted processes of Sn concentration: crystal-melt fractionation and mobilization in a fluid phase. The latter is economically more important since it would have provided the highest grades of Sn in the granite, but is unequivocally a process poorly known. Depressurisation and fluid saturation induced by anhydrous mineral crystallisation and cooling (second boiling) could both explain a strong Sn enrichment in a fluid phase and the magmatic signature of cassiterite in the central part of the granite body, but the second one predicts better the place where fluid saturation occurred: in both margins of the granite body.

Acknowledgements

The present work was financially supported by Strategic Minerals Spain, S.L. and carried out in this company and in the Department of Geology of the University of Salamanca (Spain). The authors thank to General Research Services of the University of

Salamanca for the use of laboratory facilities to perform the petrographical study. The authors wish to thank Miguel Ángel Fernández for access to the electronic microprobe facilities at the University of Oviedo (Spain). Francisco Javier López-Moro is very grateful to Professor Miguel López Plaza (University of Salamanca) for constructive criticism of a previous version of the manuscript. We gratefully appreciate careful and detailed reviews by Aleksandr Stepanov (University of Tasmania) and an anonymous reviewer. We also thank F. Pirajno for editorial handling.

Appendix A. Supplementary data

Supplementary data associated with this article can be found, in the online version, at <http://dx.doi.org/10.1016/j.oregeorev.2016.11.027>.

References

- Arribas, A., Gonzalo, F., Iglesias, M., 1982. Génesis de una mineralización asociada a una cúpula granítica: el yacimiento de estaño de Golpeas (Salamanca). *Lab. Xeol. Laxe* 3, 563–592.
- Aseri, A.A., Linnen, R.L., Dong Che, X., Thibault, Y., Holtz, F., 2015. Effects of fluorine on the solubilities of Nb, Ta, Zr and Hf minerals in highly fluxed water-saturated haplogranitic melts. *Ore Geol. Rev.* 64, 736–746.
- Bacon, C.R., 1989. Crystallization of accessory phases in magmas by local saturation adjacent to phenocrysts. *Geochim. Cosmochim. Acta* 53, 1055–1066.
- Baldwin, J.R., von Knorring, O., 1983. Compositional range of Mn-garnet in zoned granitic pegmatites. *Can. Mineral.* 21, 683–688.
- Ballouard, C., Poujol, M., Boulvais, P., Branquet, Y., Tartèse, R., Vignerresse, J.L., 2016. Nb-Ta fractionation in peraluminous granites: a marker of the magmatic-hydrothermal transition. *Geology*. <http://dx.doi.org/10.1130/G37475.1>.
- Barbony, M., Bussy, F., 2013. Petrogenesis of magmatic albite granites associated to cogenetic A-type granites: Na-rich residual melt extraction from a partially crystallized A-type granite mush. *Lithos* 177, 328–351.
- Bartels, A., Holtz, F., Linnen, R.L., 2010. Solubility of manganotantalite and manganocolumbite in pegmatitic melts. *Am. Mineral.* 95, 537–544.
- Bhalla, P., Holtz, F., Linnen, R.L., Behrens, H., 2005. Solubility of cassiterite in evolved granitic melts; effect of T, fO₂ and additional volatiles. *Lithos* 80, 387–400.
- Boynnton, W.V., 1984. Cosmochemistry of the rare earth elements: meteorite studies. In: Henderson, P. (Ed.), *Rare Earth Element Geochemistry*. Elsevier, Amsterdam, pp. 63–114.
- Boudreau, A., Simon, A., 2007. Crystallization and degassing in the Basement Sill, McMurdo Dry Valleys, Antarctica. *J. Petrol.* 48, 1369–1386.
- Cabero, M.T., Mecoleta, S., López-Moro, F.J., 2012. OPTIMASBA: a Microsoft Excel workbook to optimise the mass-balance modelling applied to magmatic differentiation processes and subsolidus overprints. *Comput. Geosci.* 42, 206–211.
- Canosa, F., Martín-Izard, A., Fuentes-Fuente, M., 2012. Evolved granitic systems as a source of rare-element deposits: the Ponte Segade case (Galicia, NW Spain). *Lithos* 153, 165–178.
- Černý, P., 1989. Exploration strategy and methods for pegmatite deposits of tantalum. In: Möller, P., Černý, P., Saupé, F. (Eds.), *Lanthanides, Tantalum and Niobium*. Springer-Verlag, Heidelberg, pp. 274–310.
- Černý, P., Blevin, P.L., Cuney, M., London, D., 2005. Granite-related ore deposits. *Econ. Geol.* 100, 337–370.
- Černý, P., Teertstra, D.K., Chapman, R., Selway, J.B., Hawthorne, F.C., Ferreira, K., Chackowsky, L.E., Wang, X.J., Meintzer, R.E., 2012. Extreme fractionation and deformation of the leucogranite – pegmatite suite at Red Cross Lake, Manitoba, Canada. *IV. Mineralogy. Can. Mineral.* 50, 1839–1875.
- Charoy, B., Noronha, F., 1996. Multistage growth of a rare-element, volatile-rich microgranite at Argemela (Portugal). *J. Petrol.* 37, 73–94.
- Chevychev, V.Y., Borodulin, G.P., Zaraisky, G.P., 2010. Solubility of columbite, (Mn, Fe)(Nb, Ta)₂O₆, in granitoid and alkaline melts at 650–850 °C and 30–400 MPa: an experimental investigation. *Geochem. Int.* 48, 456–464. <http://dx.doi.org/10.1134/S0016702910050034>.
- Chicharro, E., Martín-Crespo, T., Gómez-Ortiz, D., López-García, J.A., Oyarzun, R., Villaseca, C., 2015. Geology and gravity modeling of the Logrosán Sn–(W) ore deposits (Central Iberian Zone, Spain). *Ore Geol. Rev.* 65, 294–307.
- Claiborne, L.L., Miller, C.F., Walker, B.A., Wooden, J.L., Mazdab, F.K., Bea, F., 2006. Tracking magmatic processes through Zr/Hf ratios in rocks and Hf and Ti zoning in zircons: an example from the Spirit Mountain batholith, Nevada. *Mineral. Mag.* 70, 517–543. <http://dx.doi.org/10.1180/0026461067050348>.
- Correia Neves, J.M., Lopes Nunes, J.E., Sahama, T.G., 1974. High hafnium members of the zircon-hafnon series from the granite pegmatites of Zambezia, Mozambique. *Contrib. Mineral. Petrol.* 48, 73–80.
- Costi, H.T., Dall'agnol, R., Pichavant, M., Rämö, O.T., 2009. The peralkaline tin-mineralized Madeira cryolite albite-rich granite of Pitinga, Amazonian craton, Brazil: petrography, mineralogy and crystallization processes. *Can. Mineral.* 47, 1301–1327.

- Cuney, M., Marignac, C., Weisbrod, A., 1992. The Beauvoir topaz-lepidolite albite granite (Massif Central France). A highly specialized granite with disseminated Sn-Li-Ta-Nb-Be mineralization of magmatic origin. *Econ. Geol.* 87, 1766–1794.
- Dallmeyer, R.D., Martínez-Catalán, J.R., Arenas, R., Gil-Ibarguchi, J.L., Gutiérrez-Alonso, G., Fariás, P., Bastida, F., Aller, J., 1997. Diachronous Variscan tectonothermal activity in the NW Iberian Massif; evidence from $^{40}\text{Ar}/^{39}\text{Ar}$ dating of regional fabrics. *Tectonophysics* 277, 307–337.
- Montes, Díez., 2007. La Geología del Dominio “Ollo de Sapo” en las comarcas de Sanabria y Terra do Bolo. *Lab. Xeol. Laxe* 34, 1–494. Nova Terra.
- Díez Montes, A., Martínez Catalán, J.R., Bellido Mulas, F., 2010. Role of the Ollo de Sapo massive felsic volcanism of NW Iberia in the Early Ordovician dynamics of northern Gondwana. *Gondwana Res.* 17, 363–376.
- Dingwell, D.B., Scarfe, C.M., Cronin, D.J., 1985. The effect of fluorine on viscosities in the system $\text{Na}_2\text{O}-\text{Al}_2\text{O}_3-\text{SiO}_2$: implications for phonolites, trachytes and rhyolites. *Am. Mineral.* 70, 80–87.
- Dostal, J., Kontak, D.J., Gerel, O., Shellenutt, J.G., Fayek, M., 2015. Cretaceous ongonites (topaz-bearing albite-rich microleucogranites) from Ongon Khairkhan, Central Mongolia: products of extreme magmatic fractionation and pervasive metasomatic fluid: rock interaction. *Lithos* 236–237, 173–189.
- Eby, G.N., 1992. Chemical subdivision of the A-type granitoids: petrogenetic and tectonic implications. *Geology* 20, 641–644.
- Evans, O.E., Hanson, G.N., 1993. Accessory-mineral fractionation of rare-earth element (REE) abundances in granitoid rocks. *Chem. Geol.* 110, 69–93.
- Fiege, A., Kirchner, C., Holtz, F., Linnen, R.L., Dziony, W., 2011. Influence of fluorine on the solubility of manganotantalite (MnTa_2O_6) and manganocolumbite (MnNb_2O_6) in granitic melts – an experimental study. *Lithos* 122, 165–174.
- Fernández-Suárez, J., Gutiérrez-Alonso, G., Cox, R., Jenner, G.A., 2002. Assembly of the Armorica microplate: a strike-slip terrane delivery? Evidence from U-Pb ages of detrital zircons. *J. Geol.* 110, 619–626.
- Gutiérrez-Alonso, G., Fernández-Suárez, J., Collins, A.S., Abad, I., Nieto, E., 2005. Amazonian Mesoproterozoic basement in the core of the Ibero-Armorican Arc: $^{40}\text{Ar}/^{39}\text{Ar}$ detrital mica ages complement the zircon's tale. *Geology* 33, 637–640.
- Gutiérrez-Alonso, G., Collins, A.S., Fernández-Suárez, J., Pastor-Galán, D., González-Clavijo, E., Jourdan, F., Weil, A.B., Johnston, S.T., 2015. Dating of lithospheric buckling: $^{40}\text{Ar}/^{39}\text{Ar}$ ages of syn-orocline strike-slip shear zones in northwestern Iberia. *Tectonophysics* 643, 44–54.
- Haapala, I., 1997. Magmatic and postmagmatic processes in tin-mineralized granites: topaz-bearing leucogranite in the Eurojoki rapakivi granite stock, Finland. *J. Petrol.* 38, 1645–1659.
- Helba, H., Trumbull, R.B., Morteani, G., Khalil, S.O., Arslan, A., 1997. Geochemical and petrographic studies of Ta mineralization in the Nuweibi albite granite complex, Eastern Desert, Egypt. *Miner. Deposita* 32, 164–179.
- Herrmann, W., Berry, R.F., 2002. MINSQ – a least squares spreadsheet method for calculating mineral proportions from whole rock major element analyses. *Geochem. Explor. Environ. Anal.* 2, 361–368.
- Hoskin, P.W.O., Kinny, P.D., Wyborn, D., Chappell, B.W., 2000. Identifying accessory mineral saturation during differentiation in granitoid magmas: an integrated approach. *J. Petrol.* 9, 1365–1396.
- Huang, X.L., Wang, R.C., Chen, X.M., Hu, H., Liu, C.S., 2002. Vertical variations in the mineralogy of the Yichun topaz-lepidolite granite, Jiangxi province, Southern China. *Can. Mineral.* 40, 1047–1068.
- IGME, 1982. Mapa Geológico de España, E. 1:50,000, no 228 (Viana del Bollo). Ministerio de Industria y Energía, pp. 1–26 (in Spanish).
- Irber, V., 1999. The lanthanide tetrad effect and its correlation with K/Rb, Eu/Eu*, Sr/Eu, Y/Ho and Zr/Hf of evolving peraluminous granite suits. *Geochim. Cosmochim. Acta* 63, 489–508.
- Janoušek, V., Farrow, C.M., Erban, V., 2006. Interpretation of whole-rock geochemical data in igneous geochemistry: introducing Geochemical DataToolkit (GCDkit). *J. Petrol.* 47, 1255–1259.
- Kretz, R., 1983. Symbols for rock-forming minerals. *Am. Mineral.* 68, 277–279.
- Küster, D., 2009. Granitoid-hosted Ta mineralization in the Arabian-Nubian shield: ore deposit types, tectono-metallogenetic setting and petrogenetic framework. *Ore Geol. Rev.* 35, 68–86.
- Lehmann, B., 1994. Granite-related rare-metal mineralization: a general geochemical framework. In: Seltmann, R., Kämpf, H., Möller, P. (Eds.), *Metallogeny of Collisional Orogens*. Czech Geol Survey, Prague, pp. 342–349.
- Linnen, R.L., 1998. The solubility of Nb-Ta-Zr-Hf-W in granitic melts with Li and Li + F; constraints for mineralization in rare metal granites and pegmatites. *Econ. Geol.* 93, 1013–1025.
- Linnen, R.L., Cuney, M., 2005. Granite-related rare-element deposits and experimental constraints on Ta-Nb-W-Sn-Zr-Hf mineralization. In: Linnen, R. L., Samson, I.M. (Eds.), *Rare Element Geochemistry and Mineral Deposits*. Geological Association of Canada Short Course Notes, vol. 17. Geological Association of Canada, St. John's, NL, pp. 45–68.
- Linnen, R.L., Pichavant, M., Holtz, F., Burgess, S., 1995. The effect of fO_2 on the solubility, diffusion and speciation of tin in granitic melts at 850 °C and 2 kbar. *Geochim. Cosmochim. Acta* 59, 1579–1588.
- Linnen, R.L., Keppeler, H., 2002. Melt composition control of Zr/Hf fractionation in magmatic processes. *Geochim. Cosmochim. Acta* 66, 3293–3301. [http://dx.doi.org/10.1016/S0016-7037\(02\)00924-9](http://dx.doi.org/10.1016/S0016-7037(02)00924-9).
- López-Moro, F.J., Murciego, A., López-Plaza, M., 2007. Silurian/Ordovician asymmetrical sill-like bodies from La Codosera syncline, W Spain: a case of tholeiitic partial melts emplaced in a single magma pulse and derived from a metasomatized mantle source. *Lithos* 96, 567–590.
- López-Moro, F.J., López-Plaza, M., Romer, R.L., 2012. Generation and emplacement of shear-related highly mobile crustal melts: the synkinematic leucogranites from the Variscan Tormes Dome, Western Spain. *Int. J. Earth Sci.* 101, 1273–1298.
- López-Ruiz, J., Cebriá, J.M., 1990. *Geoquímica De Los Procesos Magmáticos*. Rueda, Madrid.
- Mangas, J., Arribas, A., 1987. Fluid inclusion study in different types of tin deposits associated with the Hercynian granites of Western Spain. *Chem. Geol.* 61, 193–208.
- Manning, D.A.C., 1981. The effect of fluorine on liquidus phase relationships in the system Qz-Ab-Or with excess water at 1 Kb. *Contrib. Mineral. Petrol.* 76, 206–215.
- Martínez-Catalán, J.R., Martínez-Poyatos, D., Bea, F., 2004. Zona Centroibérica: Introduction. In: Vera, J.A. (Ed.), *Geología de España*. Soc. Geol. España and Instituto Geológico y Minero de España, pp. 68–69.
- Massonne, H.J., Chopin, W., 1989. P-T history of the Gran Paradiso (Western Alps) metagranites based on phengite geobarometry. In: Daly, J.S., Cliff, R.A., Yardley, B.W.D. (Eds.), *Evolution of Metamorphic Belts*. Blackwell, Oxford, pp. 545–550.
- Massonne, H.J., Schreyer, W., 1987. Phengite geobarometry based on the limiting assemblage with k-feldspar, phlogopite, and quartz. *Contrib. Mineral. Petrol.* 96, 212–224.
- Melcher, F., Graupner, T., Gäbler, H.E., Sitnikova, M., Oberthür, T., Gerdes, A., Badanina, E., Chudy, T., 2016. Mineralogical and chemical evolution of tantalum–(niobium–tin) mineralisation in pegmatites and granites. Part 2: Worldwide examples (excluding Africa) and an overview of global metallogenetic patterns. *Ore Geol. Rev.* <http://dx.doi.org/10.1016/j.oregeorev.2016.03.014>.
- Middlemost, E.A.K., 1994. Naming materials in the magma/igneous rock system. *Earth Sci. Rev.* 37, 215–224.
- Miller, C.F., Stoddard, E.F., Bradsh, L.J., Dollase, W.A., 1981. Composition of plutonic muscovite: genetic implications. *Can. Mineral.* 19, 25–34.
- Montel, J.M., 1993. A model for monazite/melt equilibrium and application to the generation of granitic magmas. *Chem. Geol.* 110, 127–146.
- Montero, P., Talavera, C., Bea, F., Lodeiro, F.G., Whitehouse, M.J., 2009. Zircon geochronology of the Ollo de Sapo Formation and the age of the Cambro-Ordovician rifting in Iberia. *J. Geol.* 117, 174–191.
- Müller, A., Kearsley, A., Spratt, J., Seltmann, R., 2012. Petrogenetic implications of magmatic garnet in granitic pegmatites from southern Norway. *Can. Mineral.* 50, 1095–1115.
- Naumov, V.B., Kovalenko, V.I., Kuz'mi, M.I., Vladykin, N.V., Ivanov, G.F., 1971. Thermometric study of inclusions of melt in topaz from topaz-bearing quartz keratophyre (ongonite). *Dokl. Acad. Sci. USSR Earth Sci. Sect.* 199, 104–107.
- Peccerillo, R., Taylor, S.R., 1976. Geochemistry of Eocene calc-alkaline volcanic rocks from the Kastamonu area, northern Turkey. *Contrib. Mineral. Petrol.* 58, 63–81.
- Philpotts, A., Ague, J., 2009. *Principles of Igneous and Metamorphic Petrology*. Cambridge University Press, New York.
- Pollard, P.J., 1989. Geologic characteristics and genetic problems associated with the development of granite-hosted deposits of tantalum and niobium. In: Möller, P., Cerny, P., Saupe, F. (Eds.), *Lanthanides, Tantalum and Niobium*. Springer, New York, Berlin, Heidelberg, pp. 240–256.
- Pollard, P.J., Pichavant, M., Charoy, B., 1987. Contrasting evolution of fluorine- and boron-rich systems. *Miner. Deposita* 22, 315–321.
- Raimbault, L., Burnol, L., 1998. The Richemont rhyolite dyke (French Massif Central): a subvolcanic equivalent of rare-metal granites. *Can. Mineral.* 36, 265–282.
- Raimbault, L., Charoy, B., Cuney, M., Pollard, P.J., 1991. Comparative geochemistry of Ta-bearing granites. In: Pagel, M., Leroy, J.L. (Eds.), *Source, Transport and Deposition of Metals*. Balkema, Rotterdam, pp. 793–796.
- Rodríguez-Alonso, M.D., Peinado, M., López-Plaza, M., Franco, P., Carnicero, A., Gonzalo, J.C., 2004. Neoproterozoic-Cambrian synsedimentary magmatism in the Central Iberian Zone (Spain): geology, petrology and geodynamic significance. *Int. J. Earth Sci.* 93, 897–920.
- Rollinson, H.R., 1993. *Using Geochemical Data: Evaluation, Presentation, Interpretation*. Longman, UK.
- Rubatto, D., Hermann, J., 2007. Experimental zircon/melt and zircon/garnet trace element partitioning and implications for the geochronology of crustal rocks. *Chem. Geol.* 241, 38–61.
- Stepanov, A., Mavrogenes, J.A., Meffre, S., Davidson, P., 2014. The key role of mica during igneous concentration of tantalum. *Contrib. Mineral. Petrol.* 167, 1009–1016. <http://dx.doi.org/10.1007/s00410-014-1009-3>.
- Štemprok, M., 1990. Solubility of tin, tungsten and molybdenum oxides in felsic magmas. *Miner. Deposita* 25, 205–212.
- Taylor, J.R.P., Wall, V.J., 1992. The behavior of tin in granitoid magmas. *Econ. Geol.* 87, 403–420.
- Thomas, R., Davidson, P., Beurlen, H., 2011. Tantalite-(Mn) from the Borborema Pegmatite Province, northeastern Brazil: conditions of formation and melt and fluid-inclusion constraints on experimental studies. *Miner. Deposita* 46, 749–759.
- Valle Aguado, B., Azevedo, M.R., Schaltegger, U., Martínez Catalán, J.R., Nolan, J., 2005. U/Pb zircon and monazite geochronology of Variscan magmatism related to synconvergence extension in Central Northern Portugal. *Lithos* 82, 169–184.
- Valverde-Vaquero, P., Díez-Balda, M.A., Díez-Montes, A., Dörr, W., Escuder-Viruete, J., González-Clavijo, E., Maluski, H., Rodríguez-Fernández, L.R., Rubio, F., Villar, P., 2007. The “Hot Orogen”: Two Separate Variscan Low-Pressure Metamorphic Events in the Central Iberian Zone (Abstract 76). *Mechanics of Variscan Orogeny: A Modern View on Orogenic Research*. Geol France 2. BRGM.
- Van Lichtenvelde, M., Holtz, F., Hancher, J.M., 2010. Solubility of manganotantalite, zircon and hafnon in highly fluxed peralkaline to peraluminous pegmatitic melts. *Contrib. Mineral. Petrol.* 160, 17–32.

- Vegas, N., Aranguren, A., Cuevas, J., Tubía, J.M., 2001. Variaciones en los mecanismos de emplazamiento de los granitos del eje Sanabria-Viana do Bolo (Macizo Ibérico, España). *Boletín Geológico y Minero* 112, 79–88.
- Watson, E.B., Harrison, T.M., 1983. Zircon saturation revisited: temperature and compositional effects in a variety of crustal magma types. *Earth Planet. Sci. Lett.* 64, 295–304.
- Watson, E.B., Wark, D.A., Thomas, J.B., 2006. Crystallization thermometers for zircon and rutile. *Contrib. Mineral. Petrol.* 151, 413–433.
- Winter, J.D., 2001. *An Introduction to Igneous and Metamorphic Petrology*. Prentice Hall, New Jersey.
- Woodruff, L.G., Froelich, A.J., Belkin, H.E., Gottfried, D., 1995. Evolution of tholeiitic diabase sheet systems in the eastern United States: examples from the Culpeper Basin, Virginia–Maryland, and the Gettysburg Basin, Pennsylvania. *J. Volcanol. Geoth. Res.* 64, 143–169.
- Xiao-Lin, X., Zhen-Hua, Z., Jin-Chu, Z., Bing, R., 1999. Phase relations in albite granite-H₂O-HF system and their petrogenetic applications. *Geochem. J.* 33, 199–214.
- Yin, L., Pollard, P.J., Shouxi, H., Taylor, R.G., 1995. Geologic and geochemical characteristics of the Yichun Ta–Nb–Li deposit, Jiangxi Province, South China. *Econ. Geol.* 90, 577–585.